



Article

# Trend Shifts in Vegetation Greening and Responses to Drought in Central Asia, 1982–2022

Haiying Pei 1,2,†, Gangyong Li 3,†, Yang Wang 1,\*, Jian Peng 3, Moyan Li 4, Junqiang Yao 2,5 and Tianfeng Wei 6

- College of Grassland Science, Xinjiang Agricultural University, Urumqi 830046, China
- Institute of Desert Meteorology, China Meteorological Administration (CMA), Urumqi 830002, China
- Laboratory of Remote Sensing Monitoring of Grassland Ecosystems in Arid Zones, Grassland General Station, Xinjiang Uygur Autonomous Region, Urumqi 830049, China
- College of Geography and Tourism, Xinjiang Normal University, Urumqi 830054, China
- Field Scientific Experiment Base of Akdala Atmospheric Background, China Meteorological Administration, Akdala 836499, China
- 6 School of Architecture and Urban Planning, Lanzhou Jiaotong University, Lanzhou 730070, China
- \* Correspondence: wangyang@xjau.edu.cn; Tel.: +86-139-9925-2425
- † These authors contributed equally to this work.

### **Abstract**

Under global warming, drought frequency and its severity have risen notably, posing considerable challenges to vegetation growth. Central Asia (CA), recognized as the largest non-zonal arid zone globally, features dryland ecosystems that are particularly vulnerable to drought stress. This research examines how plant life in CA reacts to prolonged dry spells by analyzing multiple datasets, including drought indices and satellite-derived NDVI measurements, spanning four decades (1982-2022). This study also delves into the compound impact of drought, revealing how its influence on vegetation unfolds through both cumulative stress and delayed ecological responses. Based on the research results, the vegetation coverage in CA exhibited a notable rising tendency from 1982 to 1998. Specifically, it increased at a rate of  $4 \times 10^{-3}$  per year (p < 0.05). On the other hand, the direction of this trend shifted to a downward one during the period from 1999 to 2022. During this latter phase, the vegetation coverage decreased at a rate of  $-4 \times 10^{-3}$  per year (p > 0.05). Vegetation changes in the study area underwent a fundamental reversal around 1998, shifting from widespread greening during 1982–1998 to persistent browning during 1999–2022. Specifically, 98.6% of the region underwent pronounced summer drought stress, which triggered a substantial rise in vegetation browning. The vegetation response to the accumulated and lagged effects of drought varied across seasons, with summer exhibiting the strongest sensitivity, followed by spring and autumn. The lagged effect of drought predominantly influences the vegetation during the growing season and spring, affecting 59.44% and 79.27% of CA, respectively. In contrast, the accumulated effect of drought is more prominent in summer and autumn, affecting 54.92% and 56.52% of CA. These insights offer valuable guidance for ecological restoration initiatives and sustainable management of dryland ecosystems.

Keywords: Central Asia; drought; vegetation response; accumulated effect; lagged effect



Academic Editors: Nikolay S. Strigul and Runguo Zang

Received: 23 July 2025 Revised: 30 September 2025 Accepted: 10 October 2025 Published: 13 October 2025

Citation: Pei, H.; Li, G.; Wang, Y.; Peng, J.; Li, M.; Yao, J.; Wei, T. Trend Shifts in Vegetation Greening and Responses to Drought in Central Asia, 1982–2022. *Forests* **2025**, *16*, 1575. https://doi.org/10.3390/f16101575

Copyright: © 2025 by the authors. Licensee MDPI, Basel, Switzerland. This article is an open access article distributed under the terms and conditions of the Creative Commons Attribution (CC BY) license (https://creativecommons.org/licenses/by/4.0/).

# 1. Introduction

The impact of global warming on vegetation is undeniable. Under global climate change, terrestrial ecosystems serve as key regulators of energy balance and carbon

Forests 2025, 16, 1575 2 of 31

cycling [1]. Vegetation feeds back to climate change through carbon dioxide exchange and evapotranspiration [2]. As a result, at different spatio-temporal scales, vegetation changes are widely regarded as key indicators reflecting global environmental changes, and through these changes, the variation trends in climate and ecosystem can be revealed [3]. As greenhouse gas concentrations continue to rise, global warming has been exacerbated, leading to more frequent and severe droughts [4]. Climate change is persistently intensifying the spread of global arid regions. Estimates indicate that by 2100, nearly 50% of the Earth's land surface will face the threat of aridification to varying degrees [5]. Increased temperatures, rapid glacier deterioration, and more frequent and severe weather events define CA's climate change. Since the industrial era (to the present), surface temperatures in CA have risen by approximately 1.5 °C. Projections for different latitudes indicate that the warming trend will continue, with higher-latitude regions experiencing significantly greater temperature increases than mid-to-low-latitude regions. This uneven warming pattern may further alter the regional climate system [4]. Vegetation's vulnerability to drought is due to prolonged water shortages or high evapotranspiration coupled with the absence of available soil moisture, which restricts the growth of vegetation and even causes it to die [6]. On the other hand, when insufficient precipitation disrupts the soil moisture balance, the effects of drought on vegetation gradually become apparent. Therefore, an integrated assessment of vegetation and drought at different timescales (or fixed drought timescales) should be considered and will go some way toward contributing to our understanding of how vegetation responds to drought [7].

The Normalized Difference Vegetation Index (NDVI) is extensively used for gauging vegetation responses to drought-induced stress. Numerous studies have revealed a close relationship between drought indices and vegetation greenness. For example, in the Loess Plateau region, studies have found that NDVI values in areas affected by meteorological drought are often lower than those in non-drought periods in the same region, and the extent of NDVI reduction is significantly correlated with the intensity of meteorological drought [8]. Since 1982, widespread vegetation greening has been detected globally [9]. However, after 1999, a marked shift from greening to browning has been observed, largely attributed to the prolonged impact of drought combined with high temperature [10,11]. As drought is inherently a regional phenomenon, the comparison of vegetation responses between selected regions and the ecosystem is essential for revealing localized characteristics of drought [12]. Understanding how plants react to droughts is, in essence, essential for predicting the ability of ecosystems to withstand changes in climate down the line and for crafting specific strategies to conserve and adapt to these shifts [13].

Drought is essentially caused by insufficient or no precipitation in the atmosphere, leading to depletion of soil moisture and a drop in river and groundwater levels. In recent decades, multiple drought indices have been established to monitor and identify drought conditions, such as the standardized precipitation index (SPI) [14], the Palmer drought severity index (PDSI) [15], and its refined version, the Self-Calibrating PDSI (SC\_PDSI) [16], and the SPEI [17], the Thornthwaite index [18], and the P/PET quotient directly reflect the dryness or wetness of the climate. Among these, the SPI considers only precipitation across multiple timescales but fails to reflect changes in evapotranspiration demand, whereas the PDSI accounts for both water supply and demand. It serves as a classic indicator for assessing long-term soil moisture, though its fixed timescale and sensitivity to soil parameters may occasionally impose limitations. The SC-PDSI integrates rainfall, temperature, and soil wetness, capturing water availability relative to requirement, offering high precision and sensitivity to detect long-term drought [19]. The SPEI incorporates potential evapotranspiration, thereby overcoming the limitations of precipitation-only indices and enabling drought assessment across multiple timescales [17]. Therefore, this paper selects

Forests 2025, 16, 1575 3 of 31

the SPEI and SC\_PDSI drought indices. By combining the two, it is possible to more comprehensively characterize drought characteristics.

This paper uses a combination of Sen trend and MK tests. Jiang et al. used this method to analyze vegetation changes in the Yellow River basin, effectively avoiding interference from data anomalies and missing values and clearly revealing the spatio-temporal trends of vegetation changes [20]. Liu et al. employed this approach, effectively detailing vegetation dynamics within the Huai River basin [21].

Central Asia (CA) represents a critical hotspot for climate change research, where warming amplitude notably surpasses both the Northern Hemisphere and global averages [22]. With diverse topography and pronounced non-uniform vegetation distribution, this region is ecologically fragile, water-scarce, and extremely sensitive to climate change, and thus it is highly prone to drought [23,24]. Over the past decades, the region has undergone alternating wet and dry phases, which considerably affect vegetation dynamics and overall greenness levels [25]. The lagged drought effect (LDE) represents the delayed influence of past drought on present vegetation growth [26]. The accumulated drought effect (ADE) refers to the lasting, cumulative impact of past drought duration on current vegetation growth [27]. Given that 1998 constituted a key turning point in the dynamics of vegetation in CA, it is essential to analyze comparatively the differential characteristics of the impact of drought on vegetation in different seasons in the two periods before and after this point [28].

In recent years, rising temperatures, declining precipitation, and increasing evaporation have led to the accumulated drought effect on vegetation [29]. Although extensive research has explored vegetation responses in CA to drought variability, most have focused on concurrent relationships [30], while the effects of antecedent drought during different seasons on vegetation growth in the current season have largely been overlooked [31]. Tangjialeke et al. (2024) analyzed how various plant species reacted to the ADE and LDE [12]. However, prior research has concentrated on interannual variations when evaluating the previous ADE and LDE on the NDVI variability [32]. Although some studies have highlighted that drought impacts on the NDVI show pronounced seasonal differences [33], the mechanisms underlying the ADE and LDE on the seasonal scale still lack a systematic analysis. Therefore, there is a pressing need to systematically investigate the seasonal-scale characteristics of vegetation responses to the ADE and LDE in CA, which is crucial for understanding the ecological consequences of drought.

To address this deficiency, this investigation combines several drought indices (the SPEI and SC-PDSI) with satellite NDVI measurements. The aim of this study is to investigate the spatio-temporal dynamics of vegetation greenness and drought in CA over the period 1982–2022, thereby elucidating drought influences on vegetation growth. The specific objectives include the following: (1) quantifying the NDVI's seasonal shifts and spatial-temporal dynamics; (2) assessing the spatial correlation of the NDVI with drought indices; (3) assessing seasonal vegetation responses to drought; and (4) distinguishing the roles of the ADE and LDE across various seasons.

### 2. Materials and Methods

### 2.1. Study Area

The CA arid zone is located at 34.33° N–55.45° N, 46.49° E–107.29° E (Figure 1), encompassing Kazakhstan, Uzbekistan, Turkmenistan, Kyrgyzstan, Tajiki-stan, and the Xinjiang Uygur Autonomous Region, China [34]. CA terrain varies greatly, with elevations typically greater in the northeast than the northwest, including various landforms such as lowlands (e.g., the lowlands of Uzbekistan), plains (e.g., the Kazakhstan and Amu Darya Plains), and mountainous areas (e.g., the Tianshan, Pamir, and Kunlun Mountains). The

Forests 2025, 16, 1575 4 of 31

lowest elevation occurs along the Cas-pian Sea coast at -151 m, while the highest elevation exceeds 7000 m in the Tianshan Mountains [30]. CA experiences sparse precipitation, a large diurnal temperature range, and high evapotranspiration [35]. Vegetation types in this region include desert species (e.g., Haloxylon and Alhagi), grassland species (e.g., Stipa), mountain vegetation (e.g., Picea), and shrub vegetation (e.g., Anabasis salsa), as shown in Figure 1c.

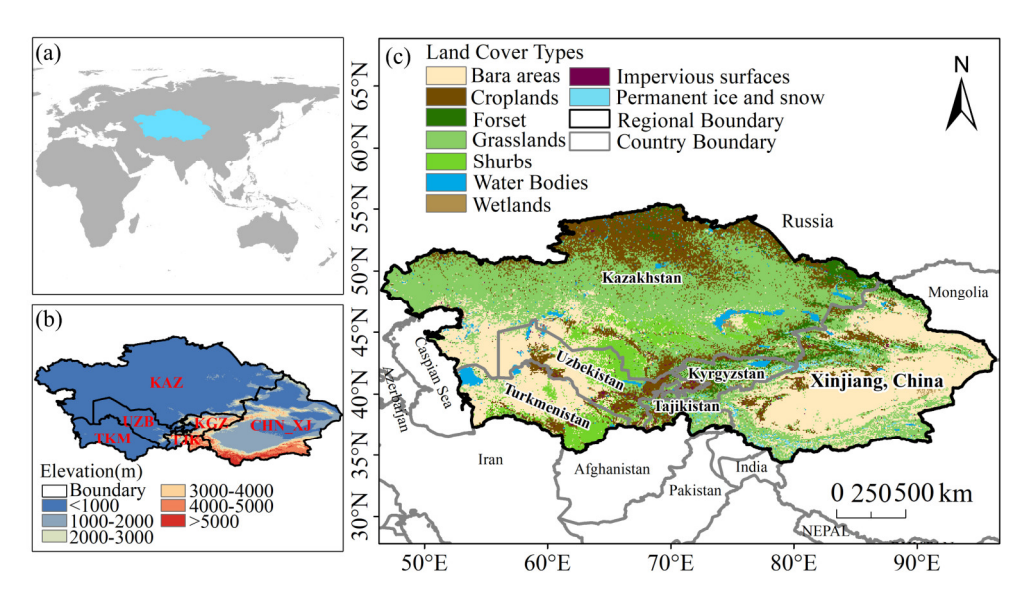


Figure 1. Study area overview: (a) site, (b) elevation map, and (c) 2020 land cover.

### 2.2. Data

This research utilizes the NDVI derived from Peking University's GIMMS-NDVI dataset (v1.2), which combines vegetation metrics from both the AVHRR and MODIS satellite imaging systems. The dataset spans the period from 1982 to 2022, offering a half-monthly temporal resolution and a 1/12° spatial resolution (https://zenodo.org/records/8253971; accessed on 24 September 2024) time resolution of 15 days [36]. In this research, the term "growing season" (GS) encompasses the period from April to September. Here is how we have divided the seasons: spring spans March through May, summer runs from June to August, autumn takes place from September to November, and winter extends from December to February. Winter is not taken into account in this paper, as the vegetation is prone to being covered by snow, and it is not possible to accurately monitor changes in vegetation dynamics. These data exhibit strong consistency with MODIS and SPOT remote sensing data [37].

To detect drought conditions, two commonly adopted indices—the SPEI and SC\_PDSI—are utilized due to their proven effectiveness in capturing spatio-temporal drought patterns [38,39]. SPEI values were sourced from the open-access Global SPEI Database (https://spei.csic.es/database.html; accessed on 7 December 2024) at a 0.5° grid resolution [22]. In general, the 3-month SPEI captures intra- and interseasonal dry and wet variations and is more sensitive to current or recent moisture stress [40]. The SC\_PDSI dataset is sourced from the University of East Anglia's CRU [41]. For consistency with the NDVI dataset, both indices are resampled to match the 1/12° spatial resolution.

Land-use classification is based on the GLC\_FCS30D data (https://zenodo.org/records/4280923; accessed on 16 January 2025) [41], which offers global coverage at a 30 m resolution for 1985–2022. Four representative years, i.e., 1990, 2000, 2010, and 2020, are selected to extract typical vegetation types.

Forests **2025**, *16*, 1575 5 of 31

### 2.3. Methods

# 2.3.1. Trend Analysis

To identify the NDVI and drought trends in CA, two trend analysis methods are employed, namely, the ordinary least squares regression [42] and the locally weighted scatterplot smoothing (LOWESS) method [43]. The LOWESS method can reveal trends or nonlinear relationships in time series. Its core principle involves applying a locally weighted regression to subsets of data points, thereby constructing a smooth curve that captures gradual trends [44]. This research utilizes the Sen's slope method [45] and the Mann-Kenfor method fir assessing vegetation and drought trends over time at the pixel level [46]. Trend assessment also employed Theil-Sen median analysis, a resilient non-parametric method, per Equation (1).

$$S = Median\left(\frac{x_j - x_i}{j - i}\right) \qquad (1982 \le i < j \le 2022) \tag{1}$$

where Median () returns the middle number in a sorted dataset, and xj and xi denote the values of the j-th and i-th terms, respectively. S > 0 represents an increasing trend, and S < 0 denotes a decreasing trend.

To evaluate the statistical significance of temporal trends, the Mann-Kendall non-parametric test is employed. It calculates a standardized test statistic (Z), where positive values signify an upward trend, while negative values reflect a declining trend.

### 2.3.2. Pearson Correlation Analysis

To quantify the relationship between the NDVI and drought, Pearson correlation analysis is conducted between the NDVI and the two drought indices: SPEI and SC\_PDSI. A *t*-test is used for testing statistical significance, and a correlation coefficient with a *p*-value of less than 0.05 is considered statistically significant. The formula is as follows.

$$r = \frac{\sum_{i=1}^{n} (x_i - \overline{x})(y_i - \overline{y})}{\sqrt{\sum_{i=1}^{n} (x_i - \overline{x})^2} \sqrt{\sum_{i=1}^{n} (y_i - \overline{y})^2}}$$
(2)

where r indicates the correlation coefficient between x and y, x is the vegetation index, y is the drought index, and n denotes the length of the time series. xi and yi represent the independent and dependent variables with time, respectively.  $\overline{x}$  and  $\overline{y}$  indicate the mean values of x and y, respectively.

### 2.3.3. Accumulated Effect of Drought on the NDVI

To gauge the vegetation response to ADE, Pearson's r was computed using monthly NDVI and SPEI datasets from 1982 to 2022 (R). For each month ( $1 \le i \le 12$ ), the corresponding SPEI value is employed to determine the correlation coefficient. The optimal accumulation duration, producing peak correlation, defines the ADE's characteristic timescale [27]. For instance, if the strongest correlation of the NDVI with the SPEI during the GS occurs on a 6-month timescale, the ADE timescale is recorded as 6 months. The calculations are shown in Equations (3) and (4).

$$R_i = \operatorname{corr}(\operatorname{NDVI}, \operatorname{SPEI}_i) \quad 1 \le i \le 12$$
 (3)

$$R_{max-cum} = max(R_i) \qquad 1 \le i \le 12 \tag{4}$$

where i denotes the typical timescale of the ADE,  $R_i$  denotes the correlation coefficient of the NDVI with the SPEI, and  $R_{\text{max-cum}}$  denotes the maximum value of  $R_i$ . Vegetation responses to drought and recovery processes occur within a finite timescale. Excessively

Forests 2025, 16, 1575 6 of 31

prolonged lag periods diminish drought signals, and extensive research indicates that drought's most pronounced effects on vegetation growth (both AED and LDE) typically concentrate within a 12-month window [47,48]. Furthermore, this timeframe effectively captures the full ecological process from transient responses to multi-annual impacts. Consequently, this study adopts a maximum 12-month period as its analytical window.

### 2.3.4. Lagged Effect of Drought on the NDVI

Likewise, the LDE is quantified through the calculation of the Pearson correlation coefficient, using monthly NDVI and SPEI datasets spanning from 1982 to 2022. Specifically, for every season and each individual pixel, the NDVI is correlated with the SPEI values that have been lagged by 1 to 12 months. The corresponding calculation formulas are presented below.

$$R_{max-lag} = max(R_i) \quad 1 \le i \le 12 \tag{5}$$

where *i* represents the lag timescale of the SPEI, *Ri* the correlation coefficient between the NDVI and the SPEI, and *Rmax-lag* the maximum value of *Ri*.

As an example, if the lag timescale is identified as 3 months, the SPEI recorded between January and June across the 1982–2022 period is correlated with the NDVI observed from April to September in the corresponding years. Given the strongest correlation aligning with optimal lag, a 3-month delay significantly shapes vegetation changes.

### 2.3.5. 5-Year Moving Average Method

In our study, the five-year moving average method was mainly used to smooth out short-term fluctuations and interannual variability in time series of vegetation indices (such as the NDVI), thereby more clearly revealing their long-term trends.

$$MA_t = \frac{Y_{t-2} + Y_{t-1} + Y_t + Y_{t+1} + Y_{t+2}}{5} \tag{6}$$

 $MA_t$  represents the moving average value in a year. Yt represents the original vegetation index value in a year. For the years inside the series (1984–2020), the centralized moving average method is used. For boundary years, an asymmetric window is used: the values for 1982 and 1983 are based on the "looking back" averages of 3 and 4 years, respectively, while the values for 2021 and 2022 are based on the "looking forward" averages of 4 and 3 years, respectively.

## 3. Results

3.1. Spatio-Temporal Variations in Vegetation in Central Asia

#### 3.1.1. Spatial Distribution Change in NDVI

NDVI directly corresponds to vegetation cover in the area; the closer the value is to 1, the higher the chlorophyll content, the more vigorous the leaf growth, and the greener the vegetation. Figure 2 presents the NDVI spatial distribution in CA during the GS and across different seasons. During the growing season, it can be found that 87.23% of CA is covered by sparse vegetation (NDVI < 0.4), primarily in the central–western areas of Kazakhstan and southern Turkmenistan. About 12.1% of CA has moderate vegetation density (NDVI of 0.4–0.6), mainly in northern Kazakhstan, Kyrgyzstan, and the Tianshan Mountains. Only 0.72% of CA falls within the NDVI range of 0.6 and 0.7, while regions with NDVI > 0.7 account for just 0.04%, concentrated in mountainous and oasis regions.

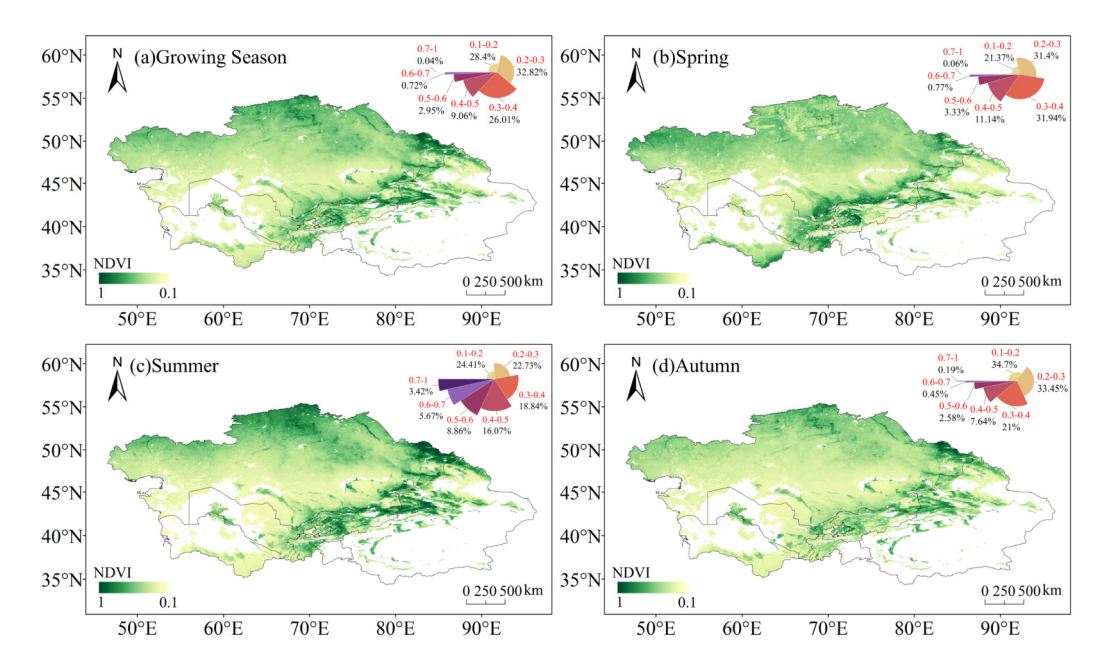


**Figure 2.** Annual spatial distribution of CA's NDVI classification levels from 1982 to 2022, including **(a)** the dry season (GS) and **(b–d)** different seasons. The top-right inset illustrates the seven-level vegetation vitality classification system [49,50], with red numbers representing the NDVI ranges for different levels and black numbers indicating the area proportion.

### 3.1.2. General Interannual Changes in NDVI

Figure 3 illustrates the NDVI temporal evolution in the GS and different seasons from 1982 to 2022. During the entire study period, the NDVI in the GS and summer shows a modest upward trend, with increasing rates of  $9 \times 10^{-5} \ \rm yr^{-1}$  and  $2 \times 10^{-4} \ \rm yr^{-1}$ , respectively. A statistically significant increase is observed in the spring NDVI at a rate of  $7 \times 10^{-4} \ \rm yr^{-1}$  (p < 0.05), while a slight decline can be found in autumn, with a rate of  $-1 \times 10^{-4} \ \rm yr^{-1}$ .

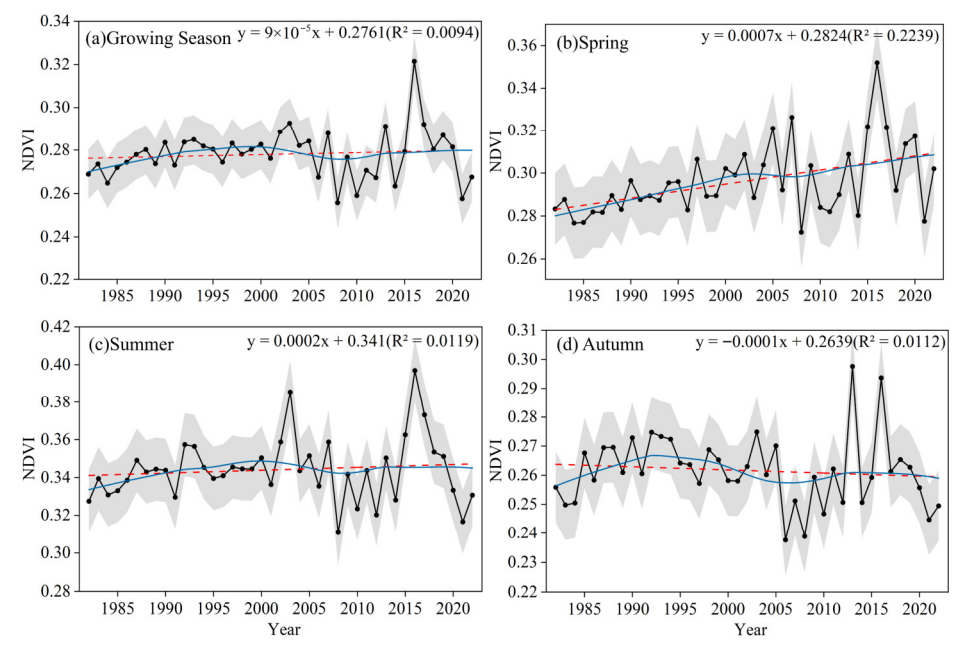


**Figure 3.** NDVI trends during (a) the GS and (b–d) different seasons in CA from 1982 to 2022. The red dashed line represents the linear trend fitted using the ordinary least squares, while the blue solid line indicates the nonlinear trend using the locally weighted scatter point smoothing method with a smoothing factor of 0.5. The shaded areas represent  $\pm 1$  standard deviation.

Forests **2025**, *16*, 1575 8 of 31

As shown in Figure 4 seasonal NDVI trends during the GS across different vegetation types in CA reveal widespread greening during 1982–2022, with the exception of shrubs. The four vegetation types—grass, shrub, coniferous forest, and broadleaf forest—cover CA from arid deserts to humid mountains and are representative of the vegetation of the region. Specifically, the increasing rate of the NDVI was the highest for broadleaf forests  $(9 \times 10^{-4} \text{ yr}^{-1})$ , followed by coniferous forests  $(3 \times 10^{-4} \text{ yr}^{-1})$ , and the smallest for grasslands  $(1 \times 10^{-4} \text{ yr}^{-1})$ . Notably, the NDVI in CA followed a three-phase fluctuation pattern characterized by "increase–decrease–increase", with pronounced interannual variations since the 21st century. Positive and negative changes in vegetation NDVI may be influenced by deforestation and environmental factors. In 2008, the NDVI reached its lowest point, while in 2016, it peaked. This phenomenon was related to the extreme drought in 2008 and the extreme precipitation in 2016 [51,52].

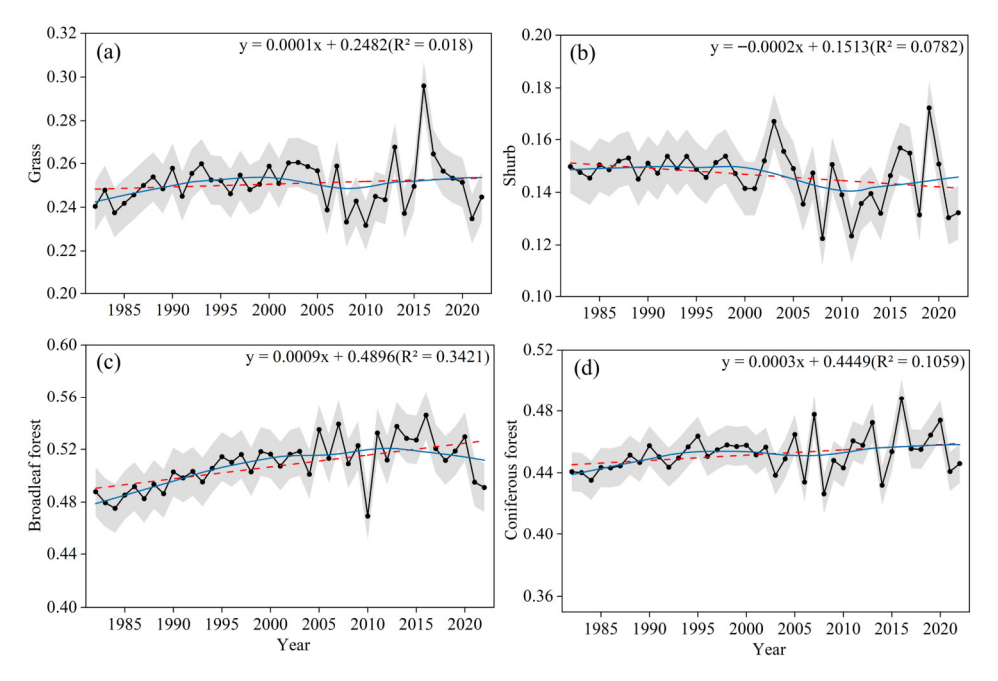


**Figure 4.** NDVI trends for different vegetation types in CA during the GS from 1982 to 2022: (a) grassland, (b) shrubs, (c) broadleaf forest, and (d) coniferous forest. The red dashed line represents the linear trend fitted using the ordinary least squares, while the blue solid line indicates the nonlinear trend using the locally weighted scatter point smoothing method with a smoothing factor of 0.5. The shaded areas represent  $\pm 1$  standard deviation.

A five-year moving average indicates an NDVI trend reversal in 1998, with inflection point maps provided in Appendix A. Since the abrupt temperature rise in 1998, CA's climate has entered a phase of heightened volatility, with evaporation rates in arid zones shifting from decline to marked increase [53]. Concurrently, a series of policies implemented during this period spurred large-scale land reclamation and persistent overgrazing, ultimately precipitating severe vegetation degradation by the early 21st century [54]. In summary, the combined effects of abrupt changes in the climate system and intensified human activities established 1998 as a pivotal turning point in the ecological evolution of CA. During 1982–1998, the NDVI in CA significantly increased (y = 0.0005x + 0.1896,  $R^2 = 0.4394$ , p < 0.05). In contrast, from 1999 to 2022, there was a significant decline in the NDVI (y = -0.0004x + 0.1931,  $R^2 = 0.106$ , p < 0.05), as presented in Figure 5a. Between 1982 and 1998, 77.6% of CA experienced an NDVI increase, while 22.4% exhibited a decreasing trend. However, during 1999–2022, 71.5% of CA showed a decreasing NDVI trend, and 28.5% displayed an increasing trend; see Figure 5. In terms of different months, except for

Forests 2025, 16, 1575 9 of 31

April, the variation trend of the NDVI in each month during 1999–2022 was consistently weaker than that in 1982–1998, showing a general decline.

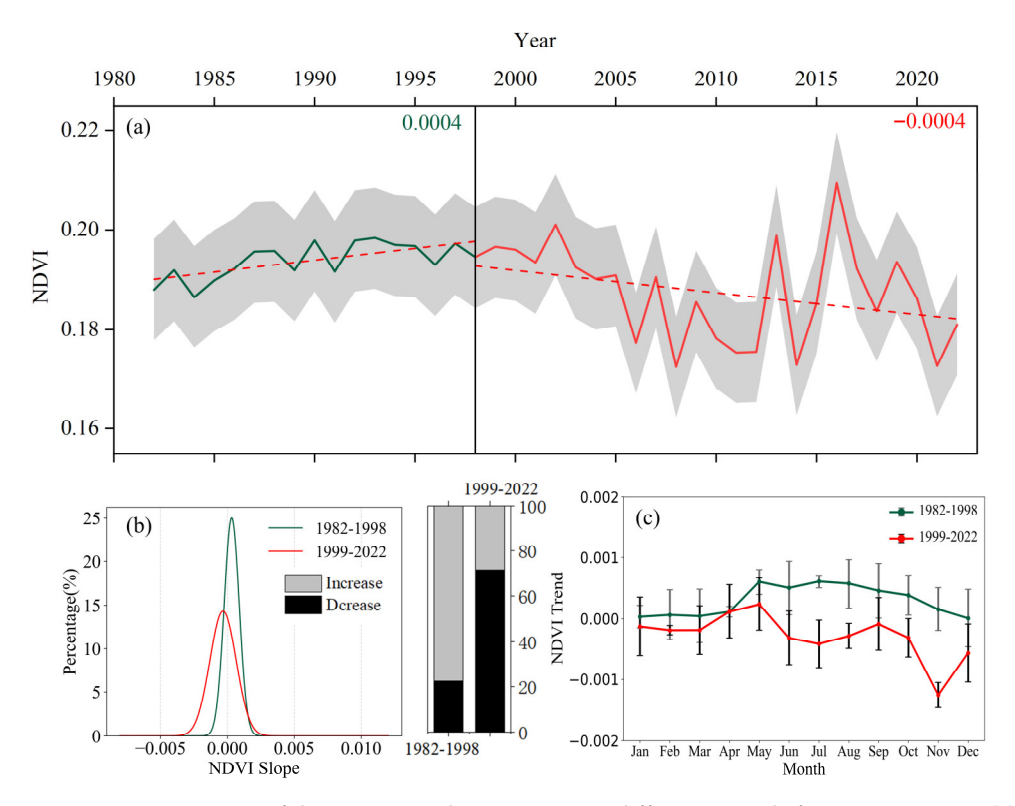


Figure 5. Comparisons of the NDVI trends in CA among different periods from 1982 to 2022: (a) time series of the NDVI during different periods (1982–1998 and 1999–2022), with numbers indicating the variation rates of the NDVI; (b) probability density functions of the normal distribution of the NDVI trend for the two periods of 1982–1998 and 1999–2022, with bars indicating the proportions of the increase and decrease in vegetation; (c) variation trend of the NDVI in each month during 1982–1998 and 1999–2022. The shaded areas in (a) and the error bars in (c) represent  $\pm 1$  standard deviation.

### 3.1.3. Spatial Distribution of NDVI Variation Trends

The NDVI variation trends in CA exhibit a remarkable uneven geographical distribution. During the GS, NDVI trends exhibit a clear east–west divide: greening in the east, browning in the west (Figure 6). Regions with statistically significant NDVI increases (p < 0.05) are primarily located in northeastern Kazakhstan, the Tianshan Mountains, the Altai Mountains, as well as the Tarim Basin. In contrast, areas west of  $70^{\circ}$  E, particularly western Kazakhstan, display significant browning trends (p < 0.05). Seasonally, over 70.6% of the region experienced NDVI increases in spring, but this trend reversed in summer, with browning occurring in 53.9% of the area, primarily along the Ili River, Syr Darya, and Amu Darya lower reaches. In autumn, browning expanded further, covering 64.5% of the CA region, and greening was only found in the Tarim River Basin and the northern slope of the Tianshan Mountains.

A comparative analysis of the spatial distributions of the NDVI trends before and after the turning point reveals that, from 1982 to 1998, the NDVI during the GS showed a distinct greening trend, with browning limited to regions near the middle–lower reaches of the Syr Darya and Lake Balkhash. For seasonal variations, greening areas in spring and autumn account for 76.8% and 75.3%, respectively, while in summer, marked browning can be found in the mid-to-lower Syr Darya; see Figure A2. During 1999–2022, significant browning was observed during the GS and across all seasons. Compared with 1982–1998, both greening and browning zones experienced clear spatial shifts. Areas with significant

Forests 2025, 16, 1575 10 of 31

browning can be found in northwestern Kazakhstan and the western Tianshan Mountains, especially in summer (Figure A3).

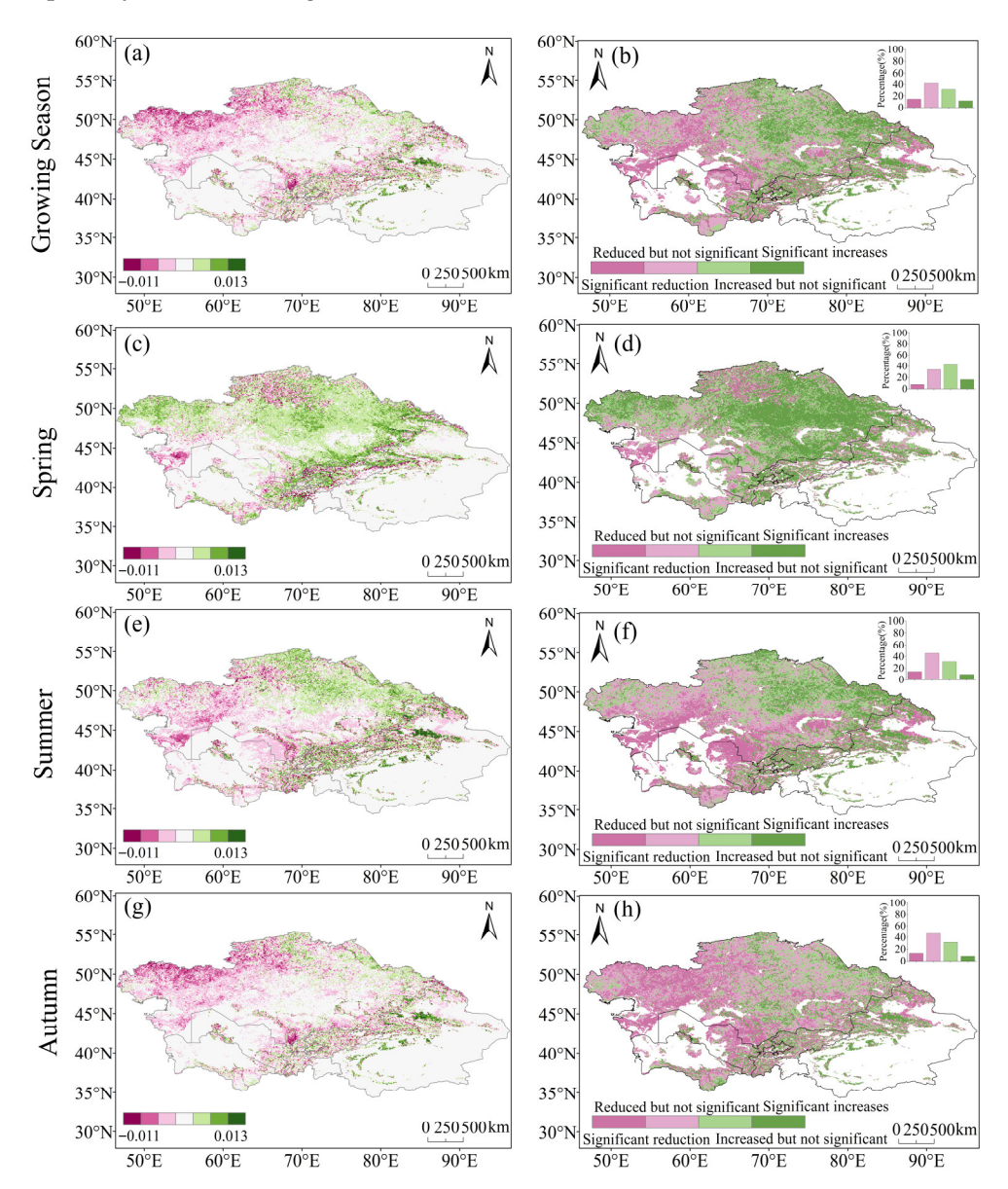


**Figure 6.** Spatial distributions of  $(\mathbf{a}, \mathbf{c}, \mathbf{e}, \mathbf{g})$  Sen's slope results and  $(\mathbf{b}, \mathbf{d}, \mathbf{f}, \mathbf{h})$  Mann-Kendall (MK) test results for NDVI trends in CA during  $(\mathbf{a}, \mathbf{b})$  the GS,  $(\mathbf{c}, \mathbf{d})$  spring,  $(\mathbf{e}, \mathbf{f})$  summer, and  $(\mathbf{g}, \mathbf{h})$  autumn from 1982 to 2022. The top-right inset shows the relative frequency (%) distributions of the significant decrease (deep pink, p < 0.05), non-significant decrease (pink), non-significant increase (green), and significant increase (deep green, p < 0.05). The blank areas in the figure are areas without vegetation.

# 3.2. Spatio-Temporal Variations in Droughts and Their Relationship with the NDVI in Central Asia

The SPEI variation from 1982 to 2022 indicates an overall aridification trend during the GS in CA (Figure 7). The aridification trend is particularly pronounced in summer, with the most widespread drought area (98.6% of the CA region), followed by autumn. In contrast, most areas experienced a wetting trend in spring. Spatially, except for humidifying trends in the mountainous regions and northeastern Kazakhstan, drying trends prevail across other regions.

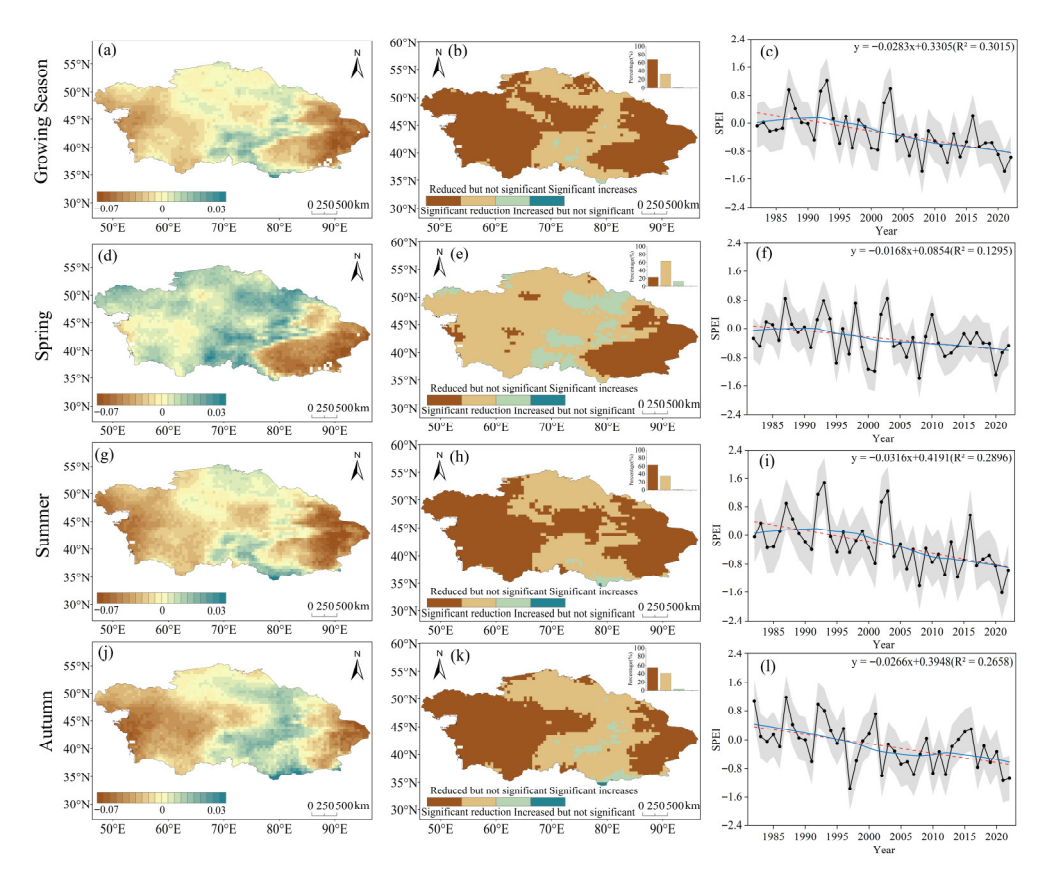


**Figure 7.** Sen's slope trends (**left panels**), MK test results (**middle panels**), and annual variation trends (**right panels**) of the SPEI in CA during (**a**–**c**) the GS, (**d**–**f**) spring, (**g**–**i**) summer, and (**j**–**l**) autumn from 1982 to 2022. The upper-right inset in the MK results shows the relative frequency (%) distribution of the significant decrease (dark brown, p < 0.05), non-significant decrease (brown), non-significant increase (green), and significant increase (dark green, p < 0.05). The red dashed line represents the linear trend fitted using the ordinary least squares, while the blue solid line indicates the nonlinear trend using the locally weighted scatter point smoothing method with a smoothing factor of 0.5. The shaded areas represent  $\pm 1$  standard deviation.

A comparative analysis of vegetation changes (Figure 6) and drought trends (Figure 7) from 1982 to 2022 shows that in southern CA, the SPEI exhibits a significant decreasing trend ( $-3.4 \times 10^{-2} \ \rm yr^{-1}$ ) in the GS, accompanied by a pronounced NDVI reduction ( $-7 \times 10^{-4} \ \rm yr^{-1}$ ). In spring, the Tianshan Mountains experienced a slight increase in the SPEI ( $1 \times 10^{-3} \ \rm yr^{-1}$ ), corresponding to a significant rise in the NDVI ( $4 \times 10^{-3} \ \rm yr^{-1}$ ). During summer, a sharp drop in the SPEI can be found around the Aral Sea ( $-4.7 \times 10^{-2} \ \rm yr^{-1}$ ), leading to a marked NDVI decrease ( $-2 \times 10^{-3} \ \rm yr^{-1}$ ). Although drought slightly decreases in autumn, the long-term drought stress leads to an intensified NDVI declining trend.

The spatial correspondences between the NDVI and the SPEI before and after the turning point reveal that regions with the increasing SPEI (humidification trend) generally exhibited vegetation greening, whereas areas with the decreasing SPEI (aridification trend) corresponded to the regions with vegetation browning. The spatial distribution of the SPEI before and after 1998 (turning point) is shown in Appendix A. This result indicates that climatic moistening supports vegetation growth, while drought stress suppresses it. Compared with the period of 1982–1998, the intensified aridification during 1999–2022 markedly increased the trend of vegetation browning across CA. Seasonally, the spatial correspondence between the NDVI and the SPEI trends was relatively consistent during 1982–1998, whereas during 1999–2022, the impact area of droughts on vegetation expanded.

Specifically, in spring, the areas with aridification extended to the margins of oases along the foothills of the Tianshan Mountains and the oasis–desert transitional zones, inhibiting early-season vegetation growth. In summer, the areas with aridification expanded into northwestern Kazakhstan, where the NDVI decline was the most pronounced. In autumn, the ADE of summer drought further amplified the NDVI reduction, leading to the further expansion of areas with significant NDVI decrease.

As shown in Figure 8, the SC\_PDSI also demonstrates a slight drying trend in CA during the GS from 1982 to 2022, with more pronounced aridification trends in summer and autumn. Through a comparison of the spatial distributions of SC\_PDSI trends before and after the turning point in 1998, it can be found a rising trend of the SC\_PDSI across most regions during 1982–1998, with the most severe drought in autumn, particularly in central Kazakhstan. However, during 1999–2022, the declining trend in the SC\_PDSI became more pronounced. The spatial distribution of SC\_PDSI before and after 1998 can be found in Appendix A.

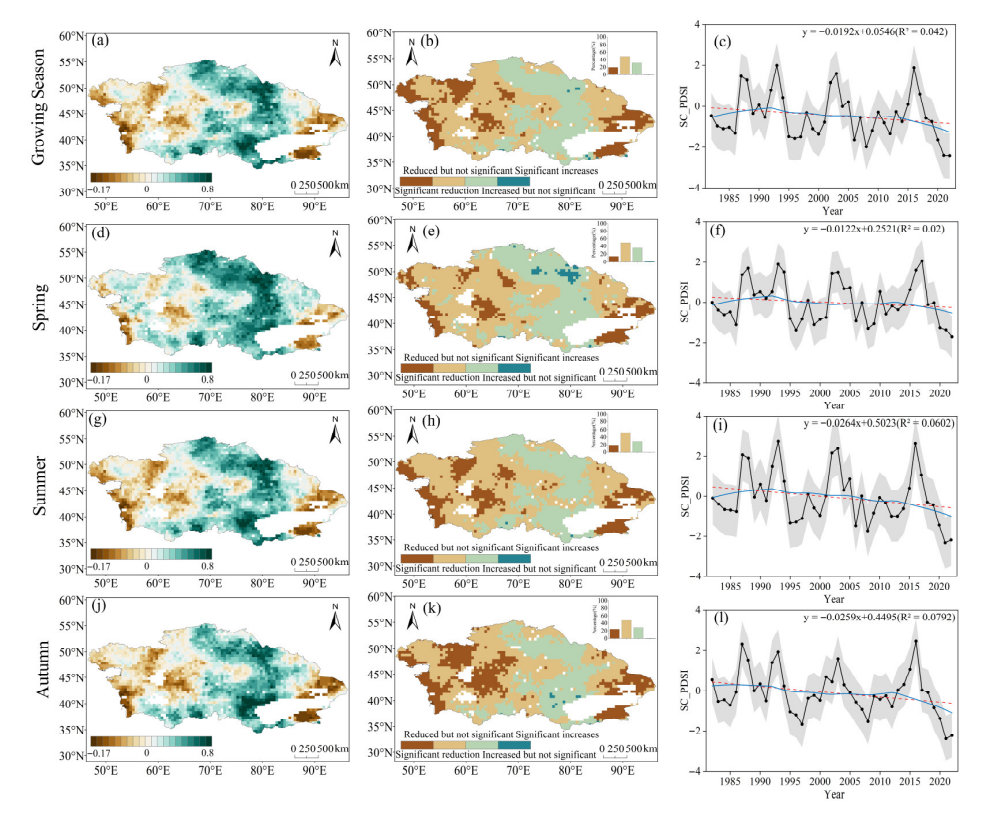


**Figure 8.** Sen's slope trends (**left panels**), MK test results (**middle panels**), and annual variation trends (**right panels**) of the SC\_PDSI in CA during (**a**–**c**) the GS, (**d**–**f**) spring, (**g**–**i**) summer, and (**j**–**l**) autumn from 1982 to 2022. The upper-right inset in the MK results shows the relative frequency (%) distribution of the significant decrease (dark brown, p < 0.05), non-significant decrease (brown), non-significant increase (green), and significant increase (dark green, p < 0.05). We have removed invalid values from the chart. The red dashed line represents the linear trend fitted using the ordinary least squares, while the blue solid line indicates the nonlinear trend using the locally weighted scatter point smoothing method with a smoothing factor of 0.5. The shaded areas represent  $\pm 1$  standard deviation.

The NDVI and SPEI exhibited notable positive correlation across all seasons from 1982 to 2022 (Figure 9). During summer, CA displays strong positive correlations exceeding 90%; conversely, spring and autumn show comparatively weaker positive relationships [55]. The analysis of correlation trends pre- and post-peak reveals a more robust positive correlation from 1999 to 2022 compared to the period from 1982 to 1998, and the regions with significant

positive correlation coefficients expanded from the oasis–desert transitional zones to most of CA (Figure 10). On a seasonal level, the NDVI–SPEI correlation in spring shifted from a spatially scattered pattern (1982–1998) to a more clustered one (1999–2022), implying that spring vegetation growth is influenced by complex interacting factors. In summer, the intensity of the positive correlation significantly increased during 1999–2022 (p < 0.05), while the correlation in autumn remained relatively weak in both periods. Comparable spatial correlation patterns are also observed between the SC\_PDSI and the NDVI. Spatial distribution maps of the SC\_PDSI correlation with the NDVI are shown in Appendix A.

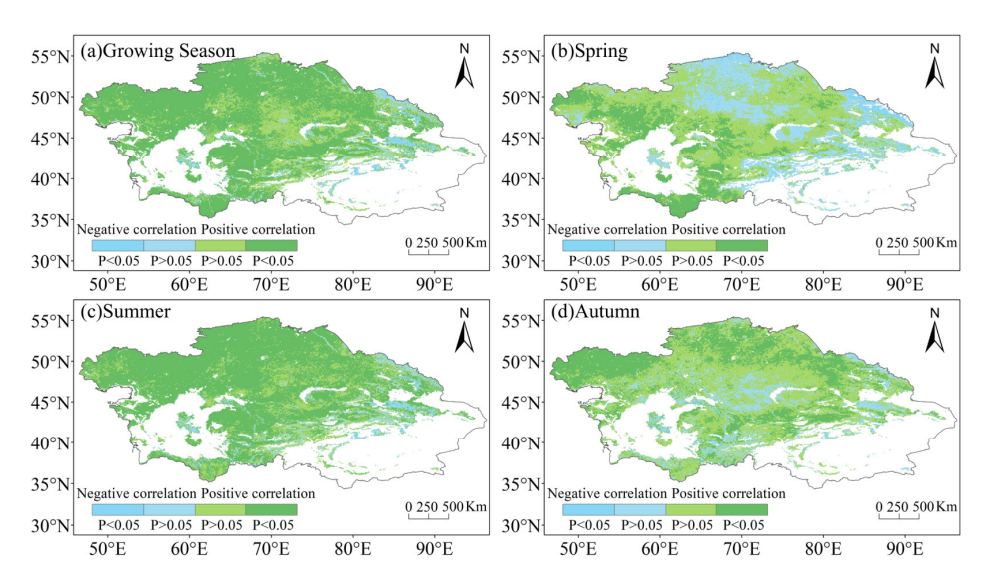


**Figure 9.** Spatial distribution of the correlation coefficient between the NDVI and the SPEI in CA during (a) the GS, (b) spring, (c) summer, and (d) autumn from 1982 to 2022. The blank areas in the figure are areas without vegetation.

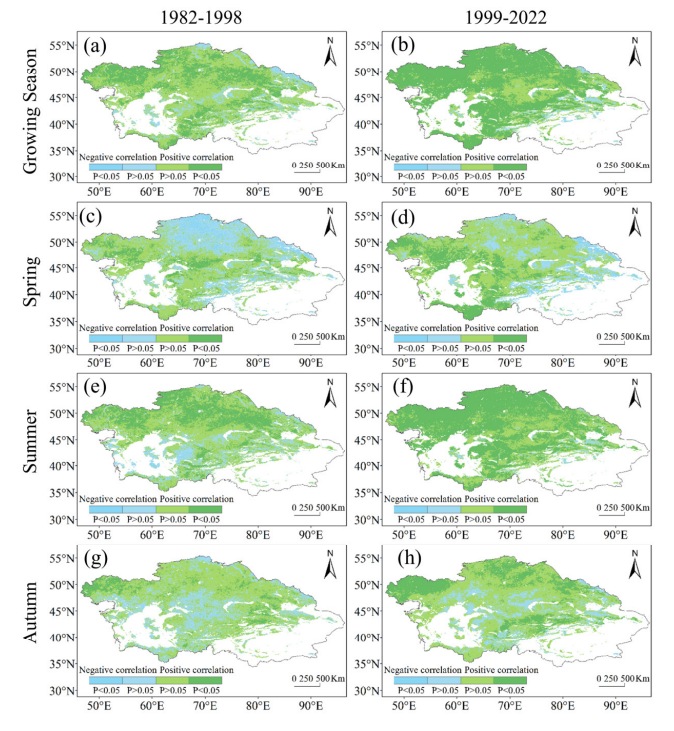


**Figure 10.** Spatial distribution of the correlation coefficient between the NDVI and the SPEI in CA during (**a**,**b**) the GS, (**c**,**d**) spring, (**e**,**f**) summer, and (**g**,**h**) autumn from (**a**,**c**,**e**,**g**) 1982 to 1998 and (**b**,**d**,**f**,**h**) 1999 to 2022. The blank areas in the figure are areas without vegetation.

### 3.3. Accumulated Effect of Drought on the Grassland NDVI

# 3.3.1. Spatial Distribution of the Accumulated Effect of Drought

The ADE varies across seasons. During the GS, 54.46% of CA exhibits a positive NDVI–SPEI correlation, primarily in northwestern Kazakhstan (Figure 11). In spring and summer, 43.65% and 88.82% of CA are significantly affected by the ADE, respectively, while in autumn, the impacted area accounts for 54.97%. Overall, the ADE on the NDVI is more pronounced in summer than in spring and autumn.

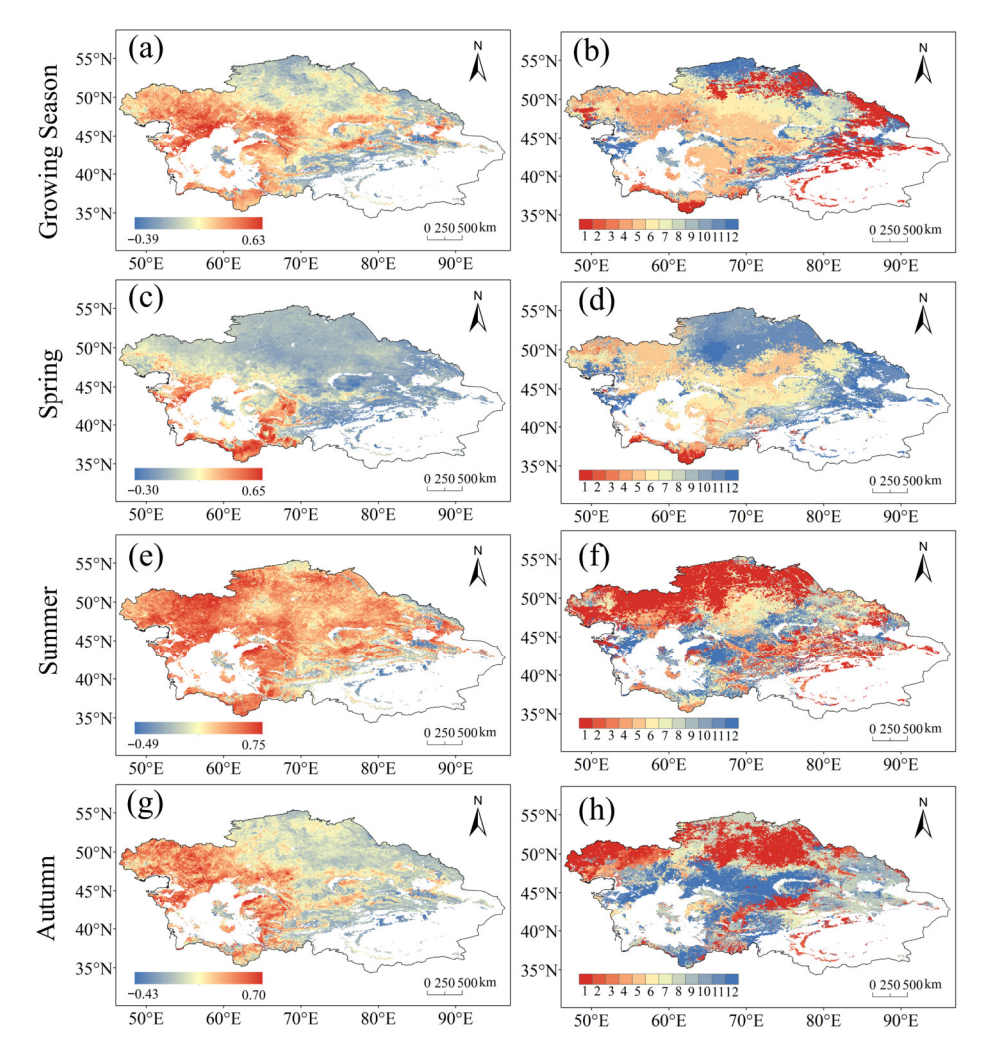


**Figure 11.** Spatial distributions of the maximum accumulated correlation coefficients (**left column**) and corresponding accumulated months (**right column**) between the NDVI and the SPEI in CA during (**a**,**b**) the GS, (**c**,**d**) spring, (**e**,**f**) summer, and (**g**,**h**) autumn from 1982 to 2022. We have removed invalid values from the chart.

The average timescale for the ADE during the GS is 6.05 months. The 5-month ADE is the greatest (22.41% of CA affected), particularly in southwestern Kazakhstan, followed by 1-month (17.39%), 6-month (13.82%), and 12-month (13.43%) effects. The droughts with a shorter-timescale ADE are mainly concentrated in northern CA and western Kazakhstan, while those with a longer-timescale ADE are observed in southern CA. In spring, the average duration of the ADE is 8.05 months, and the 5-month to 6-month ADEs exert the greatest influence (37.09% of CA). In summer, the average duration of the ADE is 5.37 months, and the droughts lasting 1–3 months have a greater impact on CA (39.55% of CA). In autumn, the corresponding average duration is 6.78 months, and the 1-month ADE has a relatively large impact (24.82% of CA).

# 3.3.2. Temporal Characteristics of the Accumulated Effect of Drought

The SPEI–NDVI relationship shows significant fluctuations across diverse temporal scales (Figure 12). Across the GS, the relationship strengthens steadily over 1–4-month periods, weakens progressively between 5–10 months, and then experiences a modest rebound in the 11–12 months. The highest correlation is observed at the timescale of 4 months (r=0.33, p<0.05), whereas the lowest occurs at 10 months (r=0.09, p<0.05). On the seasonal scale, the correlation in spring peaks on the 4-month accumulated timescale, and it peaks on the 5-month timescale in autumn. The correlation in summer is similar to that in the GS, characterized by a "double valley" pattern, and the overall correlation in summer surpasses that in spring and autumn. This result indicates that summer drought considerably contributes to the vegetation change during the GS.

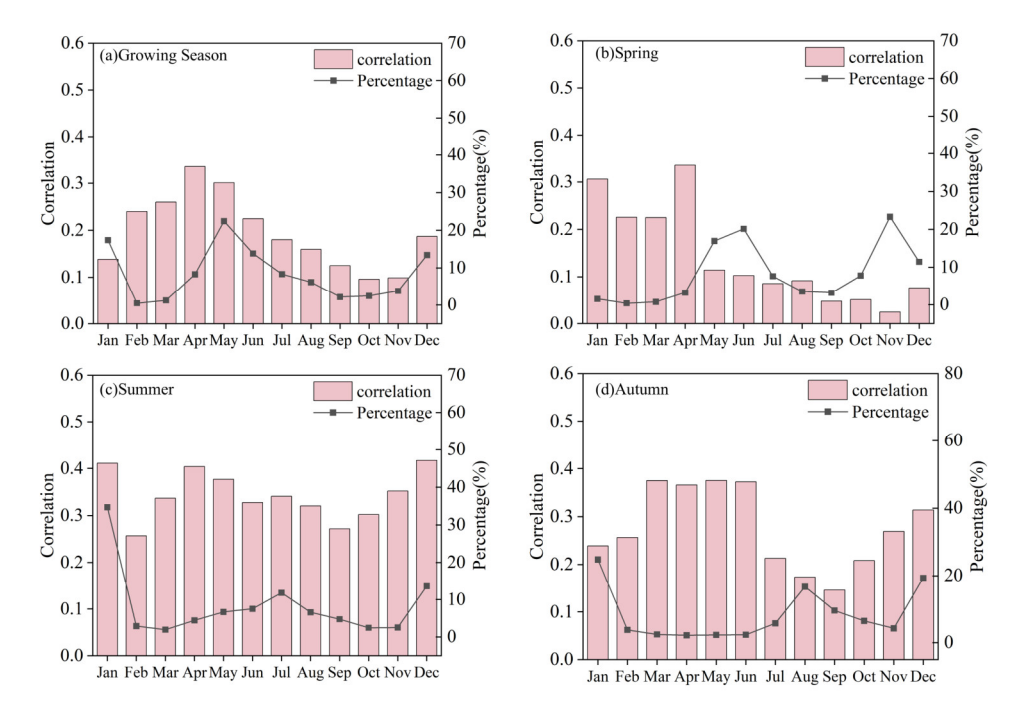


Figure 12. Correlations between the NDVI and the SPEI on the accumulated timescales of 1–12 months and the corresponding proportion of the affected area during the (a) GS, (b) spring, (c) summer, and (d) autumn from 1982 to 2022.

# 3.4. Lagged Effect of Drought on the Grassland NDVI

### 3.4.1. Spatial Distribution of the Lagged Effect of Drought

Figure 13 presents the spatial distribution of the LDE between the NDVI and the SPEI. During the GS, 75.62% of the region exhibits positive correlations between the NDVI and the lag of the SPEI, with significant correlations primarily in southwestern and southern Kazakhstan. Periodically, CA experiences a substantial LDE impact: spring (51.31%), summer (85.64%), and autumn (56.91%). The GS and summer display more pronounced delayed reactions compared to spring and autumn.

The average lagging period of drought influence on vegetation growth during the GS is estimated to be 4.59 months. A 3-month lag has the greatest impact on CA vegetation (25.64% of the region affected), mainly in central Kazakhstan, followed by 4-month (23.15% of the region affected) and 6-month lags (15.42% of the region affected). In spring, the average lagging period is also 4.59 months, and 63.89% of CA shows a lag of 4–5 months. Among them, a 4-month lag affects the largest area (34.34%). In summer, the average lagging period is 3.75 months, and the strongest effect appears at a 1-month lag (35.85% of the region affected). In autumn, the average lagging period is 5.01 months, and the 1-month

(19.52% of the region affected) and 7-month (17.33% of the region affected) lags have the most extensive impact.

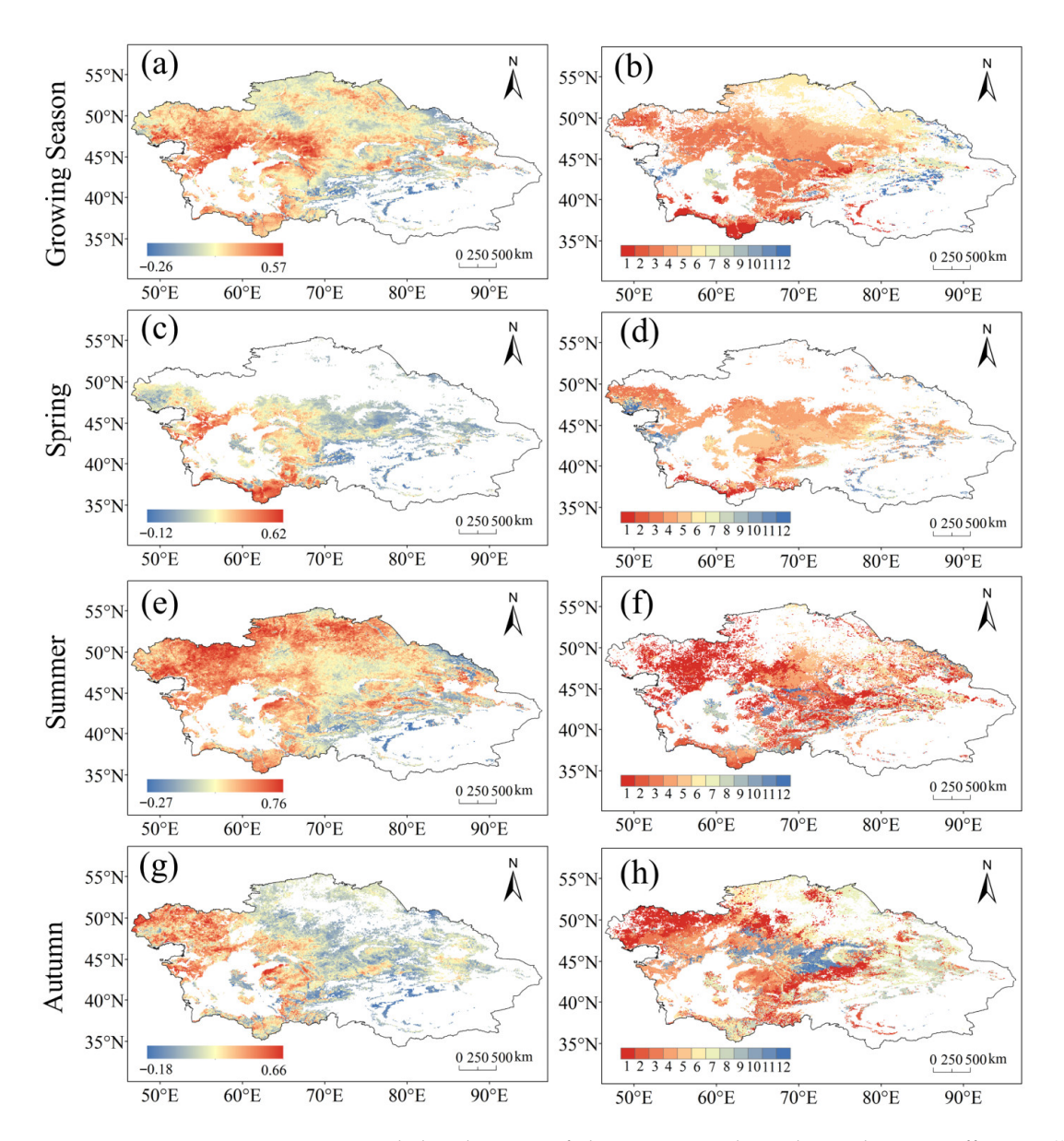


**Figure 13.** Spatial distributions of the maximum lagged correlation coefficients (**left panels**) and corresponding lag months (**right panels**) between the NDVI and SPEI during (**a**,**b**) the GS, (**c**,**d**) spring, (**e**,**f**) summer, and (**g**,**h**) autumn in CA from 1982 to 2022. We have removed invalid values from the chart.

# 3.4.2. Temporal Characteristics of the Lagged Effect of Drought

The SPEI–NDVI relationship exhibits significant variation across lag times; plants show heightened sensitivity to short-term drought lags year-round (Figure 14). Throughout the GS, the association demonstrates an erratic trend, reaching its highest point at a 3-month interval (r = 0.3, p < 0.05). Looking at the seasonal trends, springtime sees its biggest spike with a four-month delay, impacting nearly 32.67% of the region, although the connection is not super strong (r = 0.21, p < 0.05). When summer rolls around, the strongest link (r = 0.44, p < 0.05) pops up just a month later, affecting a little over a fifth of the area. In autumn, the correlation also peaks at the 1-month lag (18.85% of the area affected). Overall, summer shows the strongest and most extensive lagged responses, with a prominent peak at the 1-month lag. During the GS, vegetation dynamics are predominantly influenced by the

Forests 2025, 16, 1575 17 of 31

LDE, affecting 59.44% of CA. In spring, 79.27% of CA is affected by the LDE, while the ADE is limited to 20.72% of the region. In contrast, vegetation in summer and autumn is mainly influenced by the ADE, which affects 54.92% and 56.52% of CA, respectively.

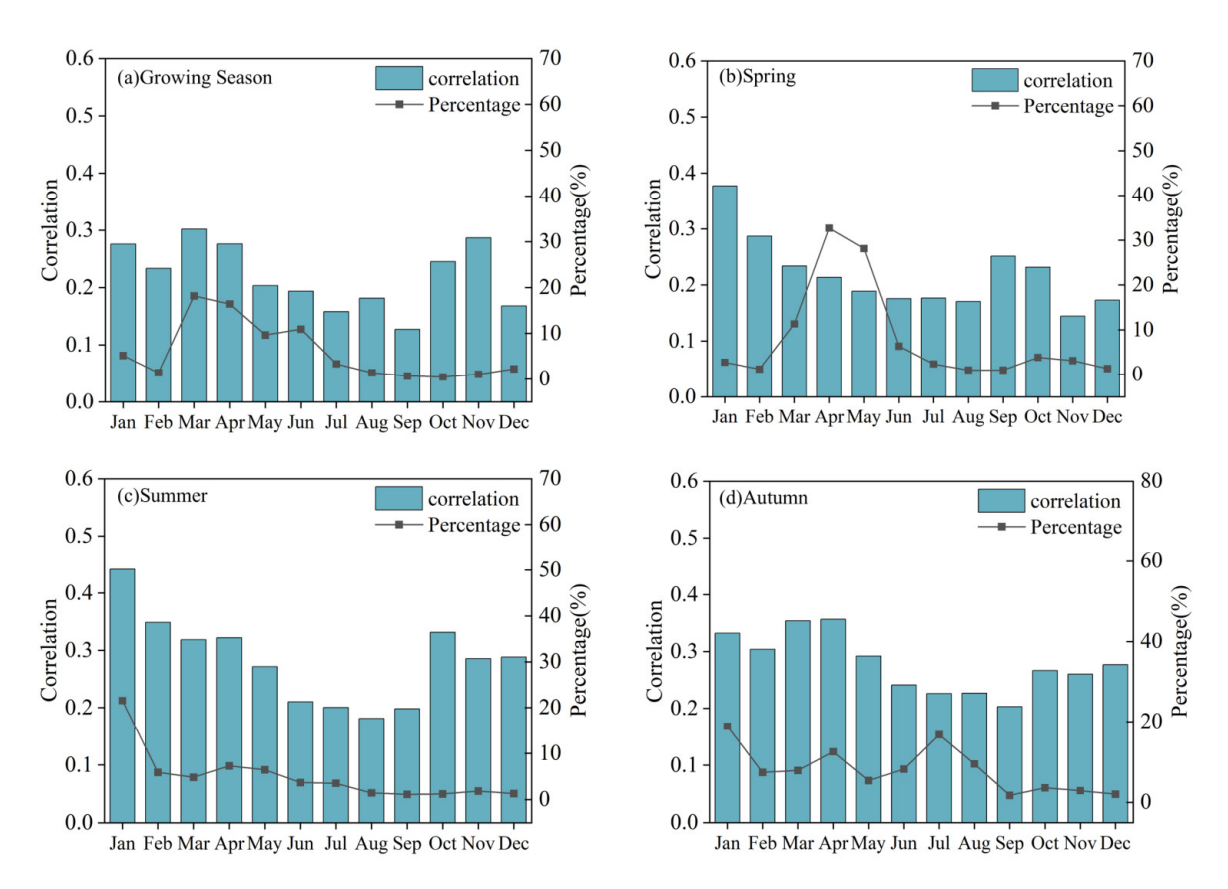


**Figure 14.** Correlations between the NDVI and the SPEI on the lag timescale of 1–12 months and the corresponding proportion of areas affected in CA during (a) the GS, (b) spring, (c) summer, and (d) autumn from 1982 to 2022.

# 4. Discussion

### 4.1. Spatio-Temporal Distributions of Vegetation and Drought

The year 1998 marks a critical turning point in vegetation dynamics across CA, aligning with findings from both global and regional studies [56]. During this period, CA's climate changed, particularly between 1982 and 1998, and CA experienced a positive phase of the North Atlantic Oscillation, which strengthened westerly moisture transport and consequently led to a precipitation increase [23]. However, after 1999, the North Atlantic Oscillation shifted to a negative phase, and coupled with the rapid warming of the Eurasian continent, it caused a distinct rise in evapotranspiration and aggravated regional droughts. Therefore, vegetation growth in CA was limited [57]. Since 1998, the overall NDVI of vegetation in CA has shown a downward trend, with an R<sup>2</sup> value of 0.3992 between 1998 and 2008. After this period, the interannual variability of the NDVI significantly increased, particularly around 2008 and 2016. These two years were marked by extreme drought and extreme precipitation events, respectively, leading to strong fluctuations in vegetation response. This fluctuation pattern highlights the sensitivity of CA ecosystems to extreme climate events and also indicates that, against the backdrop of long-term degradation, water availability remains a key factor constraining vegetation dynamics. In spring, vegetation greenness was relatively high in CA, influenced by abundant water from snowmelt [58]. In contrast, during summer, vegetation browning is severe, primarily due to intense evaporaForests 2025, 16, 1575 18 of 31

tion and long-term high temperature, which aggravated drought conditions and accelerated vegetation water loss in soil and plants, thereby suppressing vegetation growth [59].

The results of this research show that both the SPEI and SC\_PDSI display decreasing trends during 1982–2022, jointly revealing the general aridification trend in CA. This finding aligns with existing evidence indicating that the warming rate in CA surpasses the global average, further suggesting that the region is undergoing a trend toward increasing aridity [60]. On the seasonal scale, spring shows a wetting trend, while summer exhibits a drying trend. Previous studies have also suggested that early-season greening can aggravate summer drought [61–63]. Spatially, drought in CA exhibits distinct altitude dependence. Due to orographic lifting, the SPEI tends to remain relatively stable in high-altitude mountainous areas (e.g., the Tianshan Mountains and the Pamir Plateau), while in low-elevation plains and desert areas, the SPEI shows an obvious decline, forming a vertical differentiation pattern of "humid mountains and arid plains". This pattern is due to the imbalance between snowmelt supply in the highlands and evapotranspiration demand in the lowlands [64].

# 4.2. Responses of NDVI to Droughts

Our analysis also reveals distinct seasonal variations in the drought influence on vegetation through both ADE and LDE, with summer showing the most pronounced impact. This result is probably due to the accelerated evapotranspiration caused by high temperature, which accelerates vegetation water deficit accumulation [65]. Summer is the peak season of vegetation growth, with active photosynthesis and heightened sensitivity to water stress [66]. Even short-term droughts (1–3 months) can lead to evident vegetation browning. In spring, vegetation growth relies on prior soil moisture storage, requiring a longer drought period (an average of 8.05 months) to exceed ecological thresholds. This result aligns with the characteristics of snowmelt recharge and the slow consumption of deep-soil moisture in CA during spring [46]. In autumn, the LDE is more pronounced at a longer timescale (7 months), probably reflecting the adaption of vegetation, such as relying on deep root systems to access deep-soil moisture or groundwater, which can help mitigate drought stress and results in delayed responses [67].

Spatially, the short-term ADE dominates in northern CA, probably due to the rapid response of shallow-rooted grassland vegetation to instantaneous rainfall events. Conversely, in the southern regions, vegetation responses are predominantly governed by the long-term ADE, reflecting the survival strategies of desert vegetation that rely on deep groundwater or interannual water storage [68]. The southern Kazakhstani region, a hub for ADE activities, is particularly sensitive to drought accumulation due to its location in the transitional zone between arid regions and grasslands, where ecosystems are in a moisture-critical state [5]. In the northwest, the pronounced LDE is associated with the high water-holding capacity of chernozem soils, which slows the transmission of drought signals. Meanwhile, in the southern desert areas, sparse vegetation cover leads to drought responses being masked by variations in surface albedo [69].

Beyond climate change, human activities constitute the primary driver of vegetation dynamics in arid regions. Overgrazing directly leads to grassland degradation and diminished soil water retention capacity, thereby intensifying drought stress on vegetation [70]. While irrigated agriculture temporarily enhances local vegetation greenness, prolonged unsustainable water use readily induces soil salinization, ultimately undermining the overall resilience of the regional ecosystem [71]. Moreover, land-use changes such as deforestation diminish mountainous regions' water conservation capacity, potentially amplifying the ecological impacts of drought events. These anthropogenic disturbances interact synergis-

tically with climatic aridification trends, rendering vegetation responses more complex. Future research must clarify the relative contributions of each factor [72].

Based on the aforementioned research findings, the sensitivity and seasonal variations in vegetation responses to drought across CA necessitate that governments and management authorities implement differentiated, nuanced ecological conservation and water resource management policies. These should be tailored to the distinct drought response characteristics observed across different seasons, altitudes, and vegetation types. Such an approach will help mitigate the current trends of vegetation degradation and land desertification. Consequently, future investigations should emphasize vegetation responses to drought on a seasonal scale, particularly on the ADE and LDE; combine multi-scale satellite data and field measurements to assess how extreme weather affects vegetation patterns over time and space; focus on revealing differences in ecosystem resilience before and after events and identify key factors affecting resilience; develop a coupled climate-vegetation dynamics prediction model or spatio-temporal modeling to simulate the long-term impact of frequent extreme events on vegetation resilience under future scenarios. Vegetation cover has significantly degraded since 1999, indicating that ecosystems in CA arid regions are highly sensitive to climate change (such as drought), with declining ecological stability potentially leading to issues like land degradation. Vegetation responds differently to droughts in different seasons, so strategies to address drought conditions should be tailored to seasonal characteristics. Additionally, the strengthened correlation between vegetation and drought indicates that the impacts of extreme climate events are becoming increasingly significant under the backdrop of climate change, necessitating enhanced regional climate adaptation capacity building [73]. Such insights are essential for elucidating the underlying mechanisms of vegetation responses to drought and providing a scientific foundation for the sustainable development of terrestrial ecosystems.

This study reveals the impact of drought on vegetation in CA from 1982 to 2022, though it must be acknowledged that several limitations exist. Firstly, the GIMMS NDVI data employed may hinder the capture of subtle vegetation dynamics due to its limited spatial resolution (approximately 8 km) and extended synthesis cycle (15 days) in sparsely vegetated areas, alongside risks of saturation effects and interference from soil background. Secondly, the SPEI and SC-PDSI drought indices employed possess inherent limitations and fail to incorporate soil moisture data, which more directly influences vegetation growth. Furthermore, this study did not quantify the potentially significant impacts of human activities such as land-use change and agricultural management practices (e.g., irrigation), which may have dominated the observed trends in the NDVI. The designation of 1998 as a "tipping point" primarily relies on statistical trend analysis. The causal relationship with climate drivers like the North Atlantic Oscillation (NAO) and underlying physical mechanisms requires further validation through model simulations. Conclusions also lack verification by independent ground-based observations (e.g., biomass and soil moisture), and findings are predominantly centered on CA, necessitating caution when extrapolating to other arid regions.

Future research should focus on integrating higher-resolution remote sensing data (e.g., Landsat and Sentinel) with alternative vegetation indices (e.g., the EVI), while incorporating satellite-derived soil moisture products to more directly quantify water stress. Coupling climate—vegetation models could elucidate the physiological and ecological mechanisms underlying this "decoupling" phenomenon, enabling the separation of relative contributions from climate variability and human activities. Finally, multi-source data fusion analysis integrating ground-based observations with detailed land-use information represents a crucial direction for comprehensively understanding the drivers of vegetation change in CA.

Forests 2025, 16, 1575 20 of 31

# 5. Conclusions

This research delves into the plant life and water scarcity in the dry areas of CA, examining the enduring patterns and various timeframe relationships between plant density and drought from 1982 to 2022. It also investigates the seasonal nuances of the ADE and LDE on plant life. The main findings are summarized as follows.

- (1) From 1982 to 1998, CA vegetation cover experienced a significant increase, with an NDVI rising rate of  $4 \times 10^{-3} \ \rm yr^{-1}$ . However, from 1999 to 2022, the NDVI declined at the same rate of  $4 \times 10^{-3} \ \rm yr^{-1}$ . On the seasonal scale, widespread browning was evident in the GS and all seasons from 1999 to 2022, with summer showing the most pronounced vegetation degradation.
- (2) Compared with the earlier period (1982–1998), drought conditions intensified during 1999–2022. The aridification was the most marked in summer, affecting 98.6% of CA, followed by autumn and spring. As drought became more severe, the browning of vegetation accelerated. Moreover, during 1999–2022, the positive correlation of vegetation cover with drought became more pronounced, and vegetation displayed a greater sensitivity to drought. Notably, there was a stronger vegetation response to drought in the GS and summer than in spring and autumn.
- (3) Vegetation response patterns to the ADE and LDE varied across different seasons. The ADE and LDE were the most significant in summer, followed by spring and autumn. During the GS and spring, vegetation was primarily influenced by the LDE, and 59.44% and 79.27% of CA were affected, respectively. In contrast, vegetation in summer and autumn was predominantly influenced by the ADE, which affected 54.92% and 56.52% of CA, respectively.
- (4) This study contributes to understanding the seasonal patterns of cumulative and lagged mechanisms in drought's impact on vegetation, providing precise scientific grounds for ecological risk management in CA—a critical arid region. Consequently, we emphasize that future ecological restoration and management strategies should be more targeted: in the eastern mountainous areas and oasis transition zones, focus should be placed on spring water replenishment to leverage lagged effects for growth promotion; while in the arid western plains, summer drought early-warning systems and adaptive irrigation regimes grounded in short-term cumulative effects should be established. Concurrently, regional policies should advance transboundary water resource co-management and incorporate vegetation resilience indicators into land-use planning to curb ecological degradation stemming from overexploitation.

**Author Contributions:** Y.W. contributed to the formulation of the research questions; H.P. and G.L. conducted the data analysis and drafted the manuscript; J.P. and M.L. undertook data processing and result interpretation. J.Y. and T.W. oversaw the project and secured funding for this research. All authors have read and agreed to the published version of the manuscript.

**Funding:** This research was supported by the Shanghai Cooperation Organization (SCO) Science and Technology Partnership and International S&T Cooperation Program (2023E01022), the Natural Science Foundation of Xinjiang Uygur Autonomous Region (2024D01B51), and the Grassland Ecological Restoration and Management Technology Support Project (XJCYZZXZ202401).

**Data Availability Statement:** The data used and/or analyzed in this study are available from the corresponding author upon reasonable request.

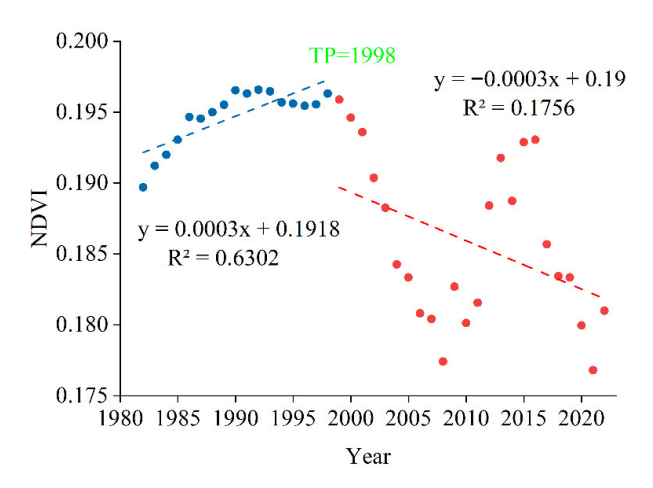
**Acknowledgments:** We sincerely acknowledge the organizations and platforms that maintain and share these datasets. Their dedication to open data access has been instrumental in supporting the progress of this research.

Conflicts of Interest: The authors declare no conflicts of interest.

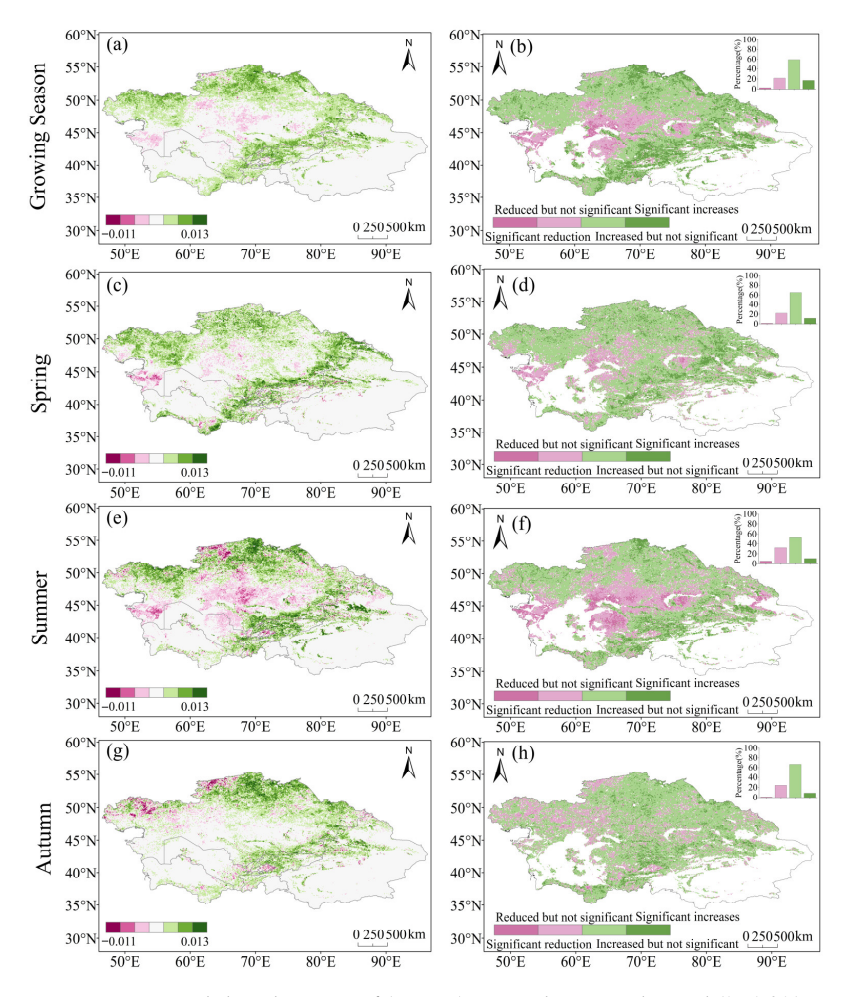
Forests 2025, 16, 1575 21 of 31

# Appendix A

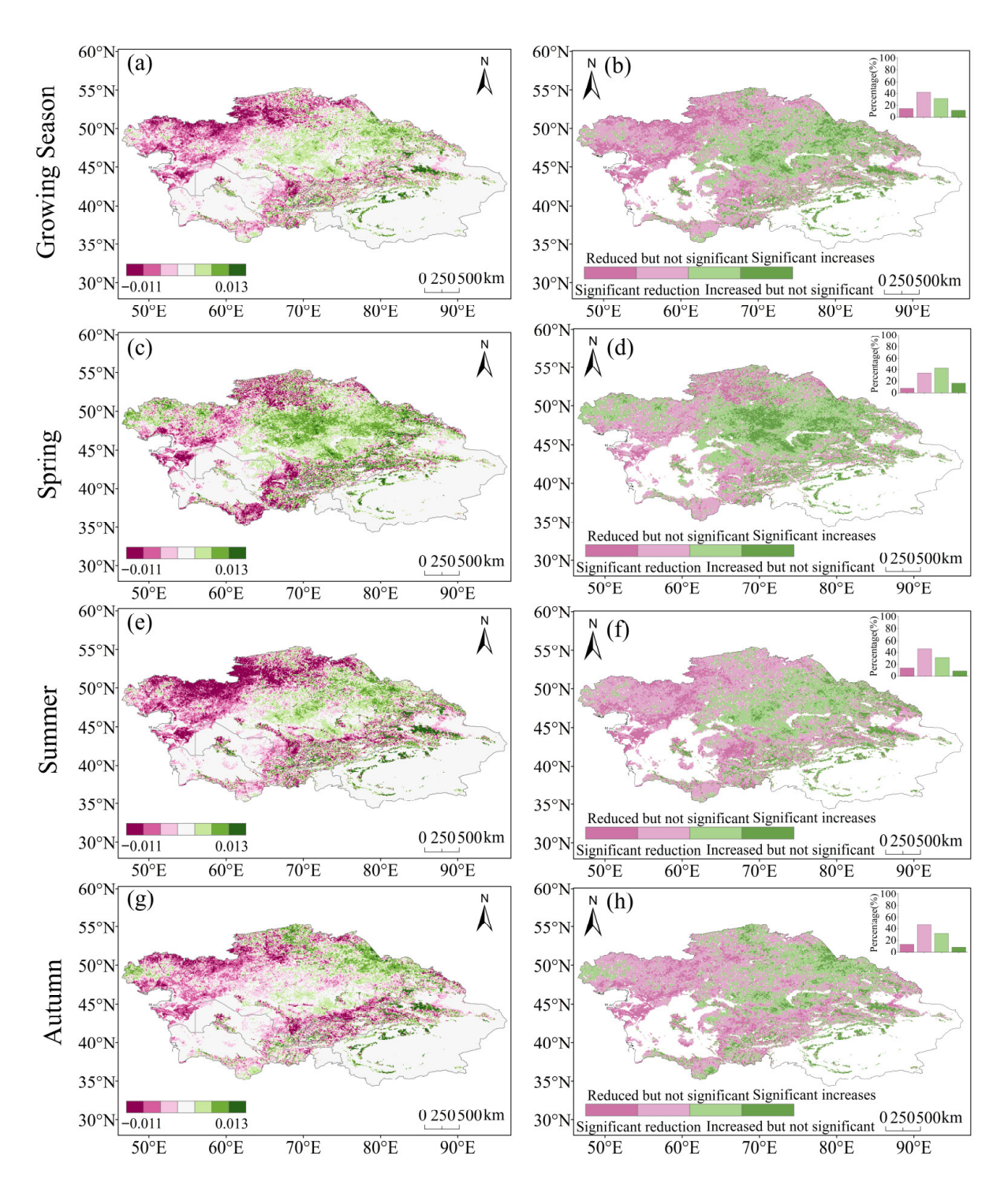
Appendix A.1 Five-Year Moving Average of the Annual NDVI



**Figure A1.** Five-year moving average of the annual NDVI. Blue and red lines indicate linear fits before and after the year with a turning point (1998).

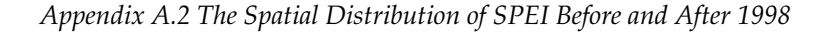


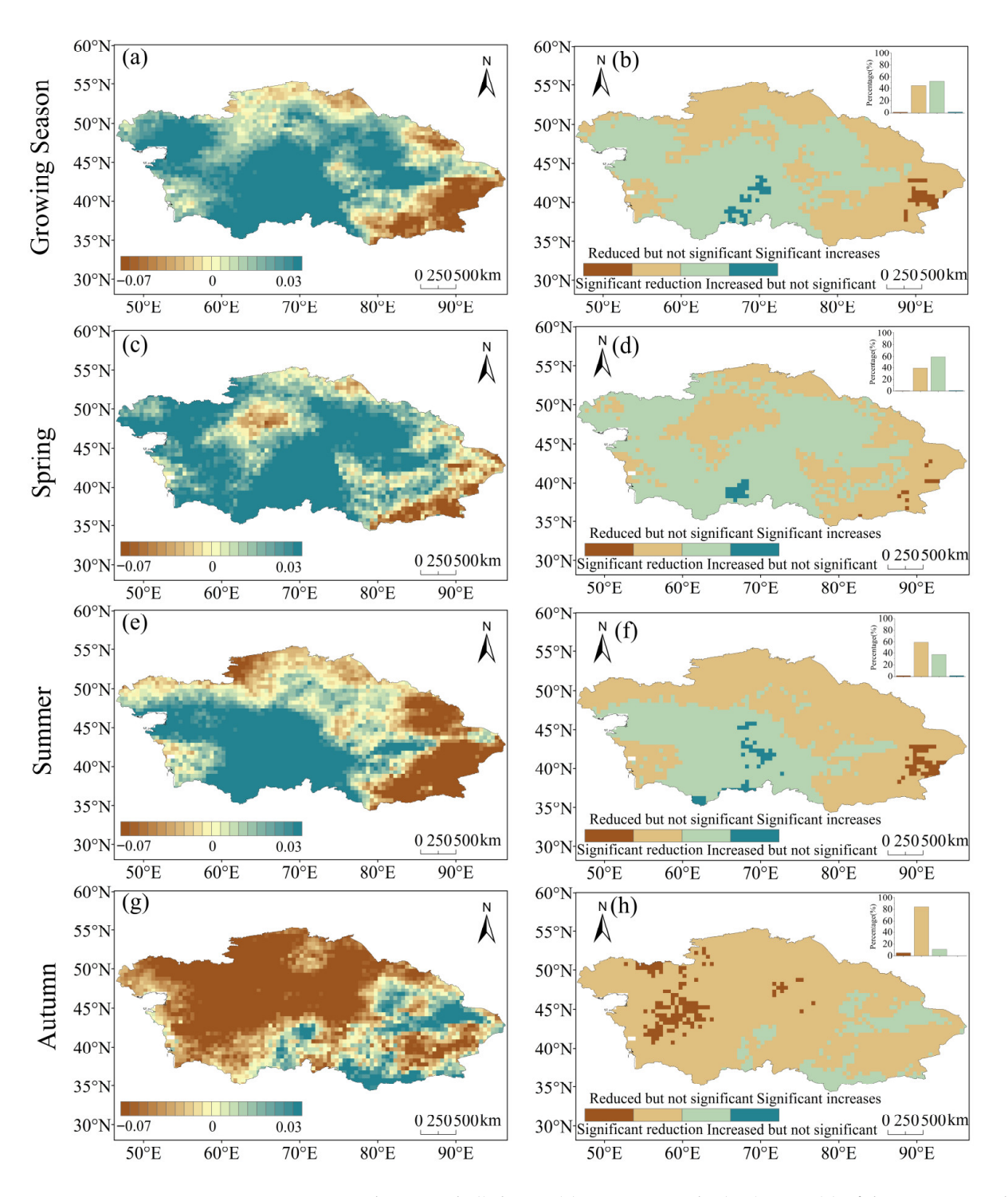
**Figure A2.** Spatial distributions of  $(\mathbf{a}, \mathbf{c}, \mathbf{e}, \mathbf{g})$  Sen's slope results and  $(\mathbf{b}, \mathbf{d}, \mathbf{f}, \mathbf{h})$  Mann-Kendall (MK) test results for NDVI trends in CA during  $(\mathbf{a}, \mathbf{b})$  the GS,  $(\mathbf{c}, \mathbf{d})$  spring,  $(\mathbf{e}, \mathbf{f})$  summer, and  $(\mathbf{g}, \mathbf{h})$  autumn from 1982 to 1998. The top-right inset shows the relative frequency (%) distributions of the significant decrease (deep pink, p < 0.05), non-significant decrease (pink), non-significant increase (green), and significant increase (deep green, p < 0.05). The blank areas in the figure are areas without vegetation.



**Figure A3.** Spatial distributions of  $(\mathbf{a}, \mathbf{c}, \mathbf{e}, \mathbf{g})$  Sen's slope results and  $(\mathbf{b}, \mathbf{d}, \mathbf{f}, \mathbf{h})$  Mann-Kendall (MK) test results for NDVI trends in CA during  $(\mathbf{a}, \mathbf{b})$  the GS,  $(\mathbf{c}, \mathbf{d})$  spring,  $(\mathbf{e}, \mathbf{f})$  summer, and  $(\mathbf{g}, \mathbf{h})$  autumn from 1999 to 2022. The top-right inset shows the relative frequency (%) distributions of the significant decrease (deep pink, p < 0.05), non-significant decrease (pink), non-significant increase (green), and significant increase (deep green, p < 0.05). The blank areas in the figure are areas without vegetation.

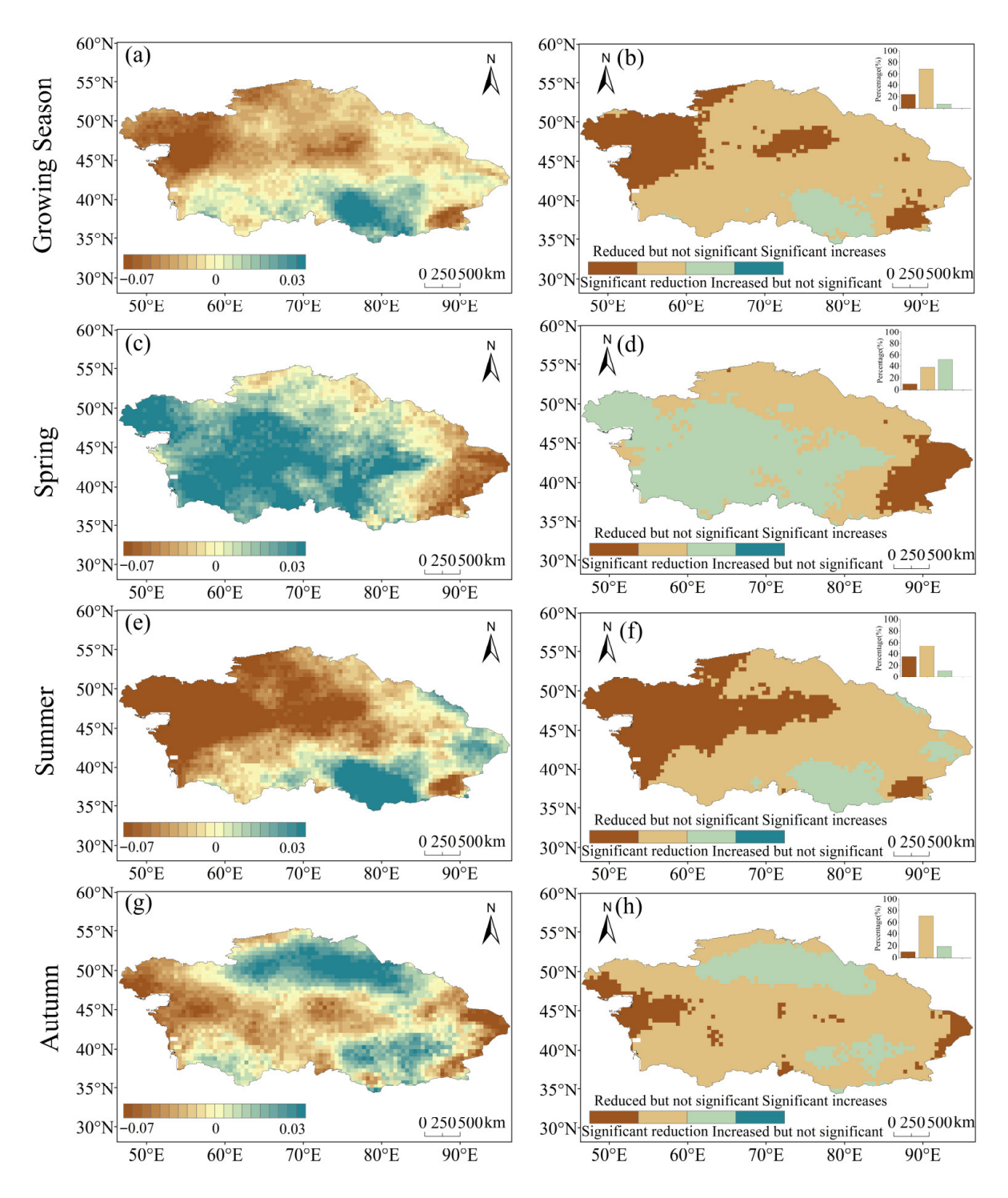
Forests 2025, 16, 1575 23 of 31





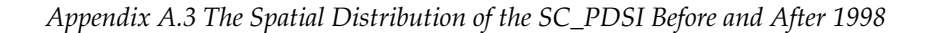
**Figure A4.** Sen's slope trends (**left panels**), MK test results (**right panels**) of the SPEI in CA during (**a**,**b**) the GS, (**c**,**d**) spring, (**e**,**f**) summer, and (**g**,**h**) autumn from 1982 to 1998. The upper-right inset in the MK results shows the relative frequency (%) distribution of the significant decrease (dark brown, p < 0.05), non-significant decrease (brown), non-significant increase (green), and significant increase (dark green, p < 0.05).

Forests 2025, 16, 1575 24 of 31



**Figure A5.** Sen's slope trends (**left panels**), MK test results (**right panels**) of the SPEI in CA during (**a,b**) the GS, (**c,d**) spring, (**e,f**) summer, and (**g,h**) autumn from 1999 to 2022. The upper-right inset in the MK results shows the relative frequency (%) distribution of the significant decrease (dark brown, p < 0.05), non-significant decrease (brown), non-significant increase (green), and significant increase (dark green, p < 0.05).

Forests **2025**, 16, 1575 25 of 31



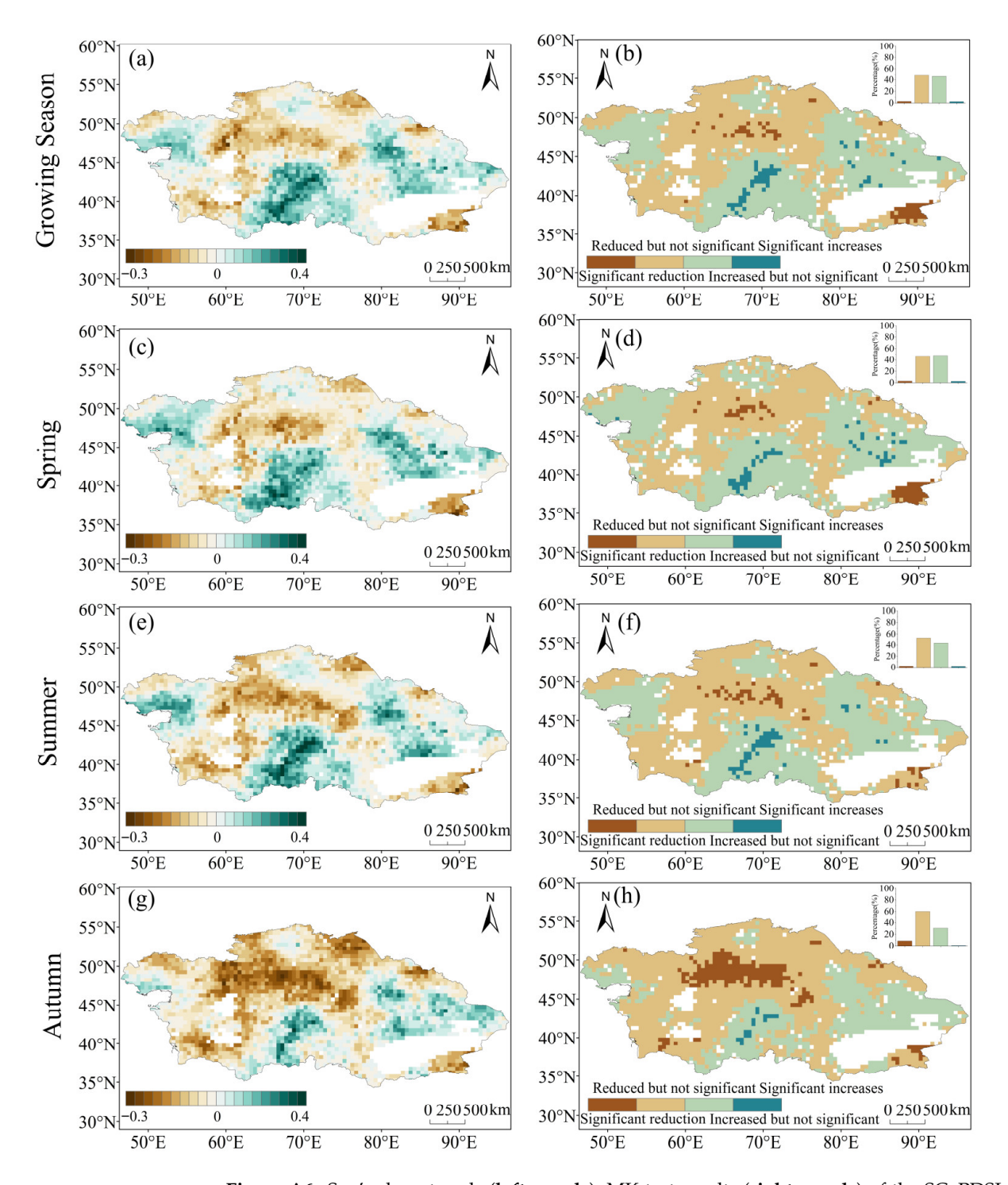


**Figure A6.** Sen's slope trends (**left panels**), MK test results (**right panels**) of the SC\_PDSI in CA during (**a,b**) the GS, (**c,d**) spring, (**e,f**) summer, and (**g,h**) autumn from 1982 to 1998. The upper-right inset in the MK results shows the relative frequency (%) distribution of the significant decrease (dark brown, p < 0.05), non-significant decrease (brown), non-significant increase (green), and significant increase (dark green, p < 0.05).

Forests **2025**, 16, 1575 26 of 31

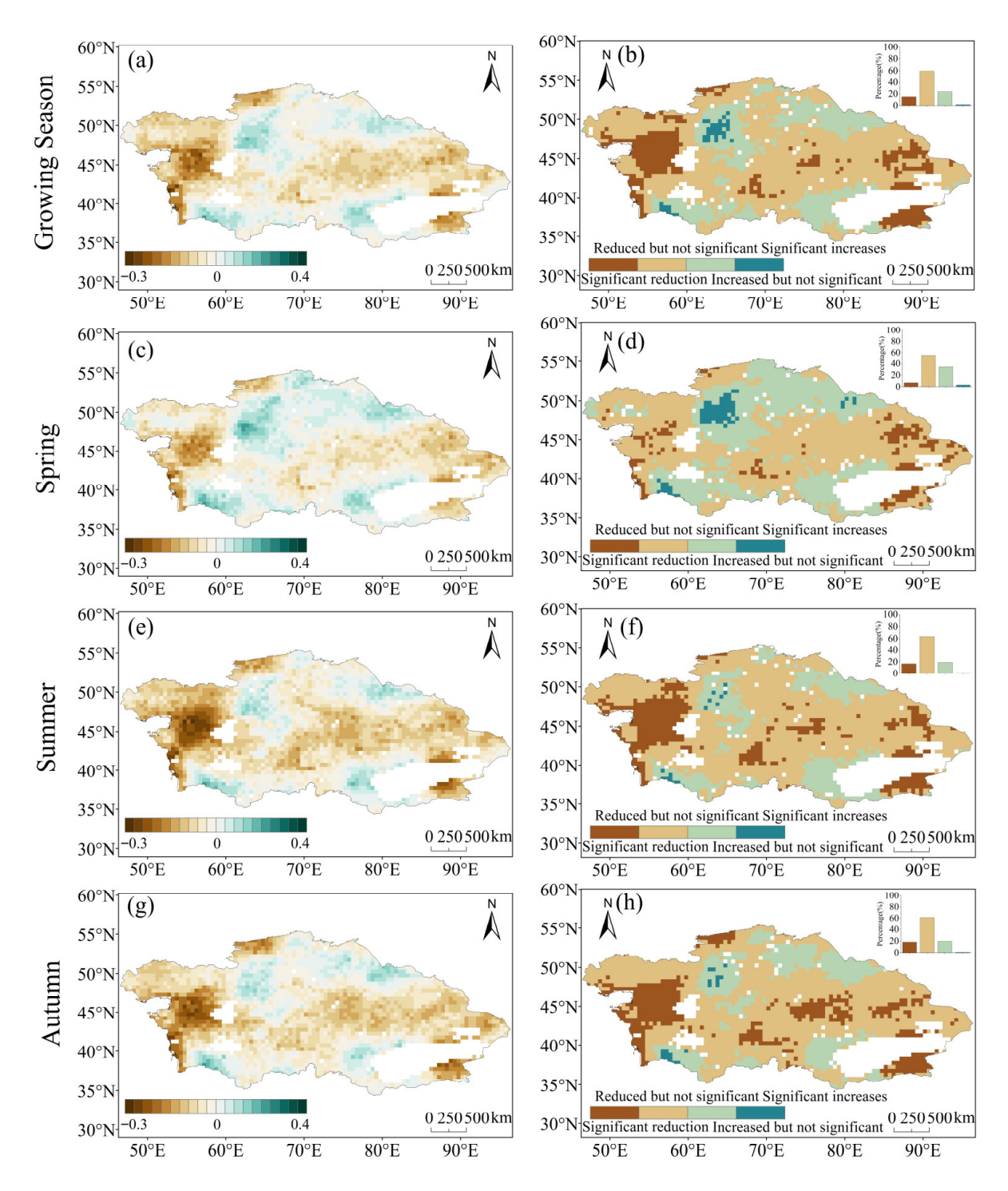


**Figure A7.** Sen's slope trends (**left panels**), MK test results (**right panels**) of the SC\_PDSI in CA during (**a**,**b**) the GS, (**c**,**d**) spring, (**e**,**f**) summer, and (**g**,**h**) autumn from 1998 to 2022. The upper-right inset in the MK results shows the relative frequency (%) distribution of the significant decrease (dark brown, p < 0.05), non-significant decrease (brown), non-significant increase (green), and significant increase (dark green, p < 0.05).

Forests **2025**, 16, 1575 27 of 31

# Appendix A.4 Spatial Distribution of the SC\_PDSI Correlation with the NDVI

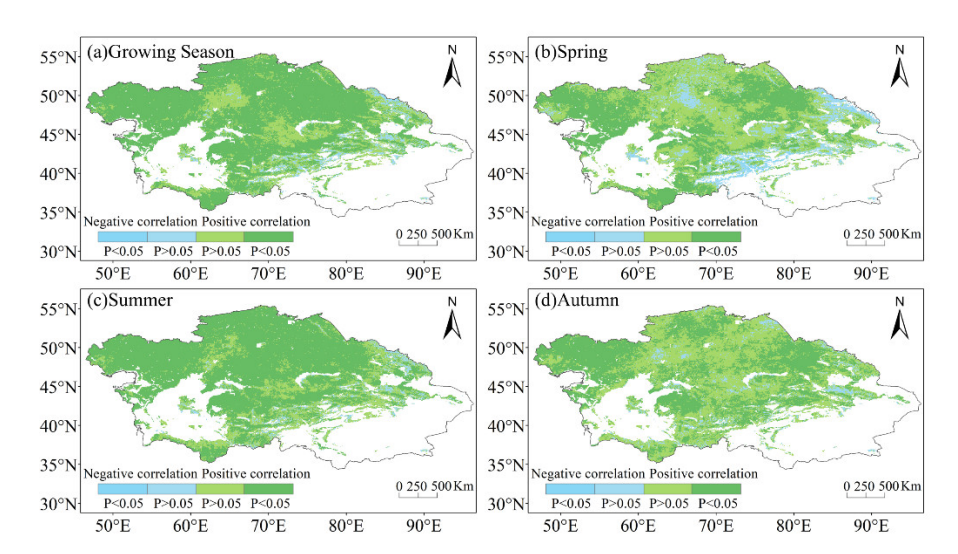


**Figure A8.** Spatial distribution of the correlation coefficient between the NDVI and the SC\_PDSI in CA during (a) the GS, (b) spring, (c) summer, and (d) autumn from 1982 to 2022. The blank areas in the figure are areas without vegetation.

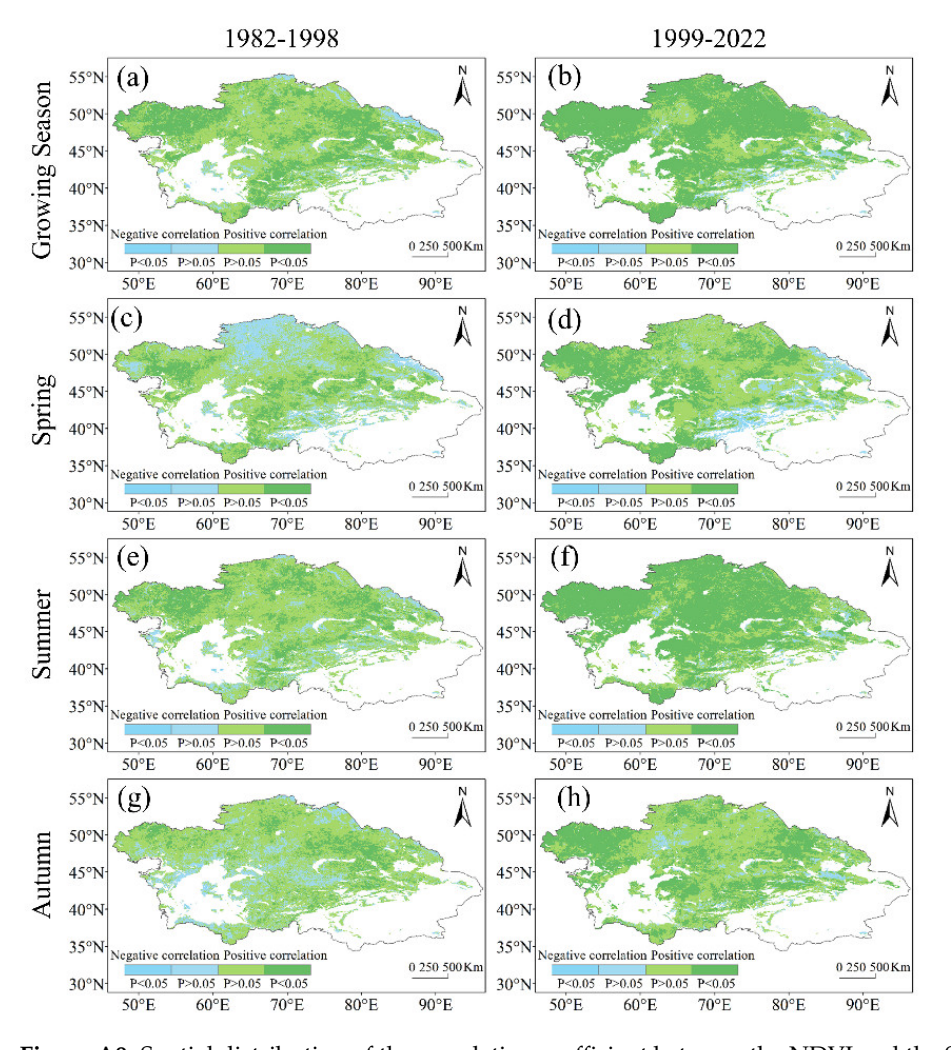


**Figure A9.** Spatial distribution of the correlation coefficient between the NDVI and the SC\_PDSI in CA during (**a**,**b**) the GS, (**c**,**d**) spring, (**e**,**f**), summer and (**g**,**h**) autumn from (**a**,**c**,**e**,**g**) 1982 to 1998 and (**b**,**d**,**f**,**h**) 1999 to 2022. The blank areas in the figure are areas without vegetation.

Forests 2025, 16, 1575 28 of 31

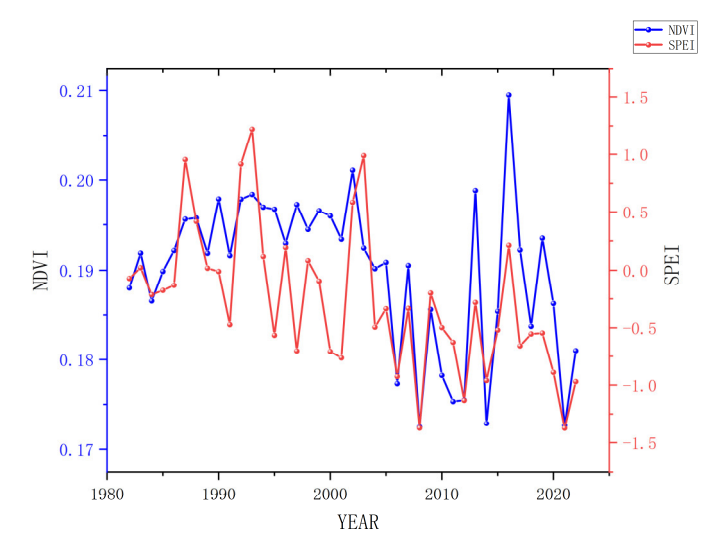


Figure A10. Correlation analysis chart between the NDVI and SPEI from 1982 to 2022.

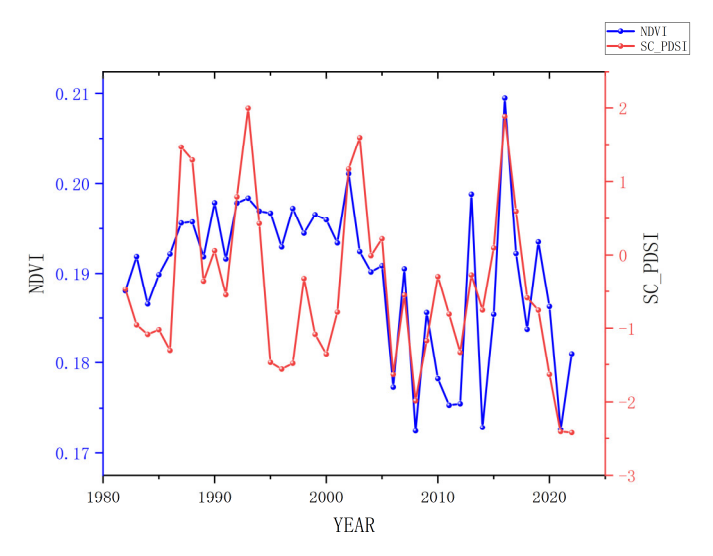


Figure A11. Correlation analysis chart between the NDVI and SC\_PDSI from 1982 to 2022.

# References

- 1. Rastetter, E.B.; Griffin, K.L.; Kwiatkowski, B.L.; Kling, G.W. Ecosystem Feedbacks Constrain the Effect of Day-to-Day Weather Variability on Land–Atmosphere Carbon Exchange. *Glob. Change Biol.* **2023**, *29*, 6093–6105. [CrossRef] [PubMed]
- 2. Piao, S.; Wang, X.; Park, T.; Chen, C.; Lian, X.; He, Y.; Bjerke, J.W.; Chen, A.; Ciais, P.; Tømmervik, H.; et al. Characteristics, Drivers and Feedbacks of Global Greening. *Nat. Rev. Earth Environ.* 2020, 1, 14–27. [CrossRef]
- 3. Taddeo, S.; Dronova, I. Indicators of Vegetation Development in Restored Wetlands. Ecol. Indic. 2018, 94, 454–467. [CrossRef]
- 4. IPCC. Climate Change 2021: The Physical Science Basis; Cambridge University Press: Cambridge, UK, 2021. [CrossRef]
- 5. Huang, J.; Yu, H.; Guan, X.; Wang, G.; Guo, R. Accelerated Dryland Expansion under Climate Change. *Nat. Clim. Change* **2016**, *6*, 166–171. [CrossRef]
- 6. Dikshit, A.; Pradhan, B.; Huete, A.; Park, H.-J. Spatial Based Drought Assessment: Where Are We Heading? A Review on the Current Status and Future. *Sci. Total Environ.* **2022**, *844*, 157239. [CrossRef]
- 7. Li, D.; An, L.; Zhong, S.; Shen, L.; Wu, S. Declining Coupling between Vegetation and Drought over the Past Three Decades. *Glob. Change Biol.* **2024**, *30*, e17141. [CrossRef]
- 8. Shi, M.; Lin, F.; Jing, X.; Li, B.; Qin, J.; Wang, M.; Shi, Y.; Hu, Y. Research on the Spatio-Temporal Changes of Vegetation and Its Driving Forces in Shaanxi Province in the Past 20 Years. *Sustainability* **2023**, *15*, 16468. [CrossRef]
- 9. Zhu, Z.; Piao, S.; Myneni, R.B.; Huang, M.; Zeng, Z.; Canadell, J.G.; Ciais, P.; Sitch, S.; Friedlingstein, P.; Arneth, A.; et al. Greening of the Earth and Its Drivers. *Nat. Clim. Change* **2016**, *6*, 791–795. [CrossRef]
- 10. Yuan, W.; Zheng, Y.; Piao, S.; Ciais, P.; Lombardozzi, D.; Wang, Y.; Ryu, Y.; Chen, G.; Dong, W.; Hu, Z.; et al. Increased Atmospheric Vapor Pressure Deficit Reduces Global Vegetation Growth. *Sci. Adv.* **2019**, *5*, eaax1396. [CrossRef]

11. Higgins, S.I.; Conradi, T.; Muhoko, E. Shifts in Vegetation Activity of Terrestrial Ecosystems Attributable to Climate Trends. *Nat. Geosci.* **2023**, *16*, 147–153. [CrossRef]

- 12. Tangjialeke, W.; Zou, J.; Ding, J.; Yahefujiang, H.; Huang, S.; Li, J. Analysis of Drought Response Thresholds and Drought-Causing Factors of Central Asian Vegetation. *Ecol. Indic.* **2024**, *169*, 112926. [CrossRef]
- 13. Zhao, A.; Zhang, A.; Cao, S.; Liu, X.; Liu, J.; Cheng, D. Responses of Vegetation Productivity to Multi-Scale Drought in Loess Plateau, China. *Catena* **2018**, *163*, 165–171. [CrossRef]
- 14. McKee, T.B.; Doesken, N.J.; Kleist, J. The Relationship of Drought Frequency and Duration to Time Scales. In Proceedings of the 8th Conference on Applied Climatology, Anaheim, CA, USA, 17–22 January 1993; pp. 179–184.
- 15. Newman, J.E.; Oliver, J.E. Palmer Index/Palmer Drought Severity Index. In *Encyclopedia of World Climatology*; Oliver, J.E., Ed.; Springer Netherlands: Dordrecht, The Netherlands, 2005; pp. 571–573. ISBN 978-1-4020-3266-0.
- 16. Wells, N.; Goddard, S.; Hayes, M.J. A Self-Calibrating Palmer Drought Severity Index. J. Clim. 2004, 17, 2335–2351. [CrossRef]
- 17. Vicente-Serrano, S.M.; Begueria, S.; Lopez-Moreno, J.I. A Multiscalar Drought Index Sensitive to Global Warming: The Standardized Precipitation Evapotranspiration Index. *J. Clim.* **2010**, 23, 1696–1718. [CrossRef]
- 18. Thornthwaite, C.W. An Approach toward a Rational Classification of Climate. Geogr. Rev. 1948, 38, 55–94. [CrossRef]
- 19. Liu, Y.; Zhu, Y.; Ren, L.; Singh, V.P.; Yang, X.; Yuan, F. A Multiscalar Palmer Drought Severity Index. *Geophys. Res. Lett.* **2017**, 44, 6850–6858. [CrossRef]
- 20. Jiang, W.; Yuan, L.; Wang, W.; Cao, R.; Zhang, Y.; Shen, W. Spatio-Temporal Analysis of Vegetation Variation in the Yellow River Basin. *Ecol. Indic.* **2015**, *51*, 117–126. [CrossRef]
- 21. Liu, Z.; Wang, H.; Li, N.; Zhu, J.; Pan, Z.; Qin, F. Spatial and Temporal Characteristics and Driving Forces of Vegetation Changes in the Huaihe River Basin from 2003 to 2018. *Sustainability* **2020**, *12*, 2198. [CrossRef]
- 22. Zhao, Z.; Hao, X.; Fan, X.; Zhang, J.; Zhang, S.; Li, X. Actual Evapotranspiration Dominates Drought in Central Asia. *Remote Sens.* **2023**, *15*, 4557. [CrossRef]
- 23. Deng, H.; Yin, Y.; Han, X. Vulnerability of Vegetation Activities to Drought in Central Asia. *Environ. Res. Lett.* **2020**, *15*, 084005. [CrossRef]
- 24. Mukherjee, S.; Mishra, A.; Trenberth, K.E. Climate Change and Drought: A Perspective on Drought Indices. *Curr. Clim. Change Rep.* **2018**, *4*, 145–163. [CrossRef]
- 25. Sun, G.-Q.; Li, L.; Li, J.; Liu, C.; Wu, Y.-P.; Gao, S.; Wang, Z.; Feng, G.-L. Impacts of Climate Change on Vegetation Pattern: Mathematical Modeling and Data Analysis. *Phys. Life Rev.* **2022**, *43*, 239–270. [CrossRef]
- 26. Braswell, B.H.; Schimel, D.S.; Linder, E.; Moore, B. The Response of Global Terrestrial Ecosystems to Interannual Temperature Variability. *Science* **1997**, *278*, 870–873. [CrossRef]
- 27. Liu, L. Cumulative Effects of Drought Have an Impact on Net Primary Productivity Stability in Central Asian Grasslands. *J. Environ. Manag.* **2023**, 344, 118734. [CrossRef]
- 28. Nie, X.; Zhang, X.; Hao, F.; Li, X.; De Boeck, H.J.; Fu, Y.H. Turning Points in Vegetation Phenology Trends and Their Relationship to Climate in Arid Central Asia. *J. Geophys. Res. Biogeosci.* **2024**, *129*, e2023JG007989. [CrossRef]
- Sheffield, J.; Wood, E.F. Projected Changes in Drought Occurrence under Future Global Warming from Multi-Model, Multi-Scenario, IPCC AR4 Simulations. Clim. Dyn. 2008, 31, 79–105. [CrossRef]
- 30. Jiang, L.; Jiapaer, G.; Bao, A.; Guo, H.; Ndayisaba, F. Vegetation Dynamics and Responses to Climate Change and Human Activities in Central Asia. *Sci. Total Environ.* **2017**, 599, 967–980. [CrossRef] [PubMed]
- 31. Sun, Y.; Chen, X.; Yu, Y.; Qian, J.; Wang, M.; Huang, S.; Xing, X.; Song, S.; Sun, X. Spatiotemporal Characteristics of Drought in Central Asia from 1981 to 2020. *Atmosphere* **2022**, *13*, 1496. [CrossRef]
- 32. Yang, M.; Zou, J.; Ding, J.; Zou, W.; Yahefujiang, H. Stronger Cumulative than Lagged Effects of Drought on Vegetation in Central Asia. *Forests* **2023**, *14*, 2142. [CrossRef]
- 33. Vicente-Serrano, S.M.; Gouveia, C.; Julio Camarero, J.; Begueria, S.; Trigo, R.; Lopez-Moreno, J.I.; Azorin-Molina, C.; Pasho, E.; Lorenzo-Lacruz, J.; Revuelto, J.; et al. Response of Vegetation to Drought Time-Scales across Global Land Biomes. *Proc. Natl. Acad. Sci. USA* 2013, 110, 52–57. [CrossRef] [PubMed]
- 34. Yuan, X.; Wang, W.; Cui, J.; Meng, F.; Kurban, A.; De Maeyer, P. Vegetation Changes and Land Surface Feedbacks Drive Shifts in Local Temperatures over Central Asia. *Sci. Rep.* **2017**, *7*, 3287. [CrossRef]
- 35. Hao, X.; Fan, X.; Zhao, Z.; Zhang, J. Spatiotemporal Patterns of Evapotranspiration in Central Asia from 2000 to 2020. *Remote Sens.* **2023**, *15*, 1150. [CrossRef]
- 36. Li, M.; Cao, S.; Zhu, Z.; Wang, Z.; Myneni, R.B.; Piao, S. Spatiotemporally Consistent Global Dataset of the GIMMS Normalized Difference Vegetation Index (PKU GIMMS NDVI) from 1982 to 2022. *Earth Syst. Sci. Data* **2023**, 15, 4181–4203. [CrossRef]
- 37. Liu, Y.; Li, Z.; Chen, Y.; Li, Y.; Li, H.; Xia, Q.; Kayumba, P.M. Evaluation of Consistency among Three NDVI Products Applied to High Mountain Asia in 2000–2015. *Remote Sens. Environ.* **2022**, 269, 112821. [CrossRef]

Forests 2025, 16, 1575 30 of 31

38. Keersmaecker, W.D.; Lhermitte, S.; Tits, L.; Honnay, O.; Somers, B.; Coppin, P. A Model Quantifying Global Vegetation Resistance and Resilience to Short-term Climate Anomalies and Their Relationship with Vegetation Cover. *Glob. Ecol. Biogeogr.* **2015**, 24, 507–610. [CrossRef]

- 39. Mondal, S.K.; An, S.-I.; Min, S.-K.; Jiang, T.; Su, B. Enhanced Soil Moisture-Temperature Coupling Could Exacerbate Drought under Net-Negative Emissions. *npj Clim. Atmos. Sci.* **2024**, *7*, 265. [CrossRef]
- 40. Liu, S.; Tian, Y.; Yin, Y.; An, N.; Dong, S. Temporal Dynamics of Vegetation NDVI and Its Response to Drought Conditions in Yunnan Province. *Acta Ecol. Sin.* **2016**, *36*, 4699–4707. [CrossRef]
- 41. Zhang, X.; Liu, L.; Chen, X.; Gao, Y.; Xie, S.; Mi, J. GLC\_FCS30: Global Land-Cover Product with Fine Classification System at 30m Using Time-Series Landsat Imagery. *Earth Syst. Sci. Data* **2021**, *13*, 2753–2776. [CrossRef]
- 42. Hou, W.; Gao, J.; Wu, S.; Dai, E. Interannual Variations in Growing-Season NDVI and Its Correlation with Climate Variables in the Southwestern Karst Region of China. *Remote Sens.* **2015**, *7*, 11105–11124. [CrossRef]
- 43. Basarin, B.; Lukić, T.; Pavić, D.; Wilby, R.L. Trends and Multi-annual Variability of Water Temperatures in the River Danube, Serbia. *Hydrol. Process.* **2016**, *30*, 3105–3336. [CrossRef]
- 44. Zhang, Q.; Harman, C.J.; Ball, W.P. An Improved Method for Interpretation of Riverine Concentration-Discharge Relationships Indicates Long-Term Shifts in Reservoir Sediment Trapping. *Geophys. Res. Lett.* **2016**, 43, 10215–10224. [CrossRef]
- 45. Sen, P.K. Estimates of the Regression Coefficient Based on Kendall's Tau. J. Am. Stat. Assoc. 1968, 63, 1379–1389. [CrossRef]
- 46. Mann, H.B. Nonparametric Tests against Trend. Econometrica 1945, 13, 245–259. [CrossRef]
- 47. Ji, L.; Peters, A.J. Assessing Vegetation Response to Drought in the Northern Great Plains Using Vegetation and Drought Indices. *Remote Sens. Environ.* **2003**, *87*, 85–98. [CrossRef]
- 48. Piao, S.; Nan, H.; Huntingford, C.; Ciais, P.; Friedlingstein, P.; Sitch, S.; Peng, S.; Ahlström, A.; Canadell, J.G.; Cong, N.; et al. Evidence for a Weakening Relationship between Interannual Temperature Variability and Northern Vegetation Activity. *Nat. Commun.* 2014, 5, 5018. [CrossRef]
- 49. Tong, S.; Zhang, J.; Ha, S.; Lai, Q.; Ma, Q. Dynamics of Fractional Vegetation Coverage and Its Relationship with Climate and Human Activities in Inner Mongolia, China. *Remote Sens.* **2016**, *8*, 776. [CrossRef]
- 50. Xu, H.; Wang, X.; Yang, T. Trend Shifts in Satellite-Derived Vegetation Growth in Central Eurasia, 1982–2013. *Sci. Total Environ.* **2017**, 579, 1658–1674. [CrossRef]
- 51. Xu, H.; Wang, X.; Zhang, X. Decreased Vegetation Growth in Response to Summer Drought in Central Asia from 2000 to 2012. *Int. J. Appl. Earth Obs. Geoinf.* **2016**, 52, 390–402. [CrossRef]
- 52. van Vliet, M.T.H.; Sheffield, J.; Wiberg, D.; Wood, E.F. Impacts of Recent Drought and Warm Years on Water Resources and Electricity Supply Worldwide. *Environ. Res. Lett.* **2016**, *11*, 124021. [CrossRef]
- 53. Foster, G.; Rahmstorf, S. Global Temperature Evolution 1979–2010. Environ. Res. Lett. 2011, 6, 44022. [CrossRef]
- 54. Li, Z.; Chen, Y.; Shen, Y.; Liu, Y.; Zhang, S. Analysis of Changing Pan Evaporation in the Arid Region of Northwest China. *Water Resour. Res.* **2013**, *49*, 2205–2212. [CrossRef]
- 55. Yuan, B.; Guo, S.; Zhang, X.; Mu, H.; Cao, S.; Xia, Z.; Pan, X.; Du, P. Quantifying the Drought Sensitivity of Vegetation Types in Northern China from 1982 to 2022. *Agric. For. Meteorol.* **2024**, *359*, 110293. [CrossRef]
- Li, Z.; Chen, Y.; Li, W.; Deng, H.; Fang, G. Potential Impacts of Climate Change on Vegetation Dynamics in Central Asia. J. Geophys. Res. Atmos. 2015, 120, 12345–12356. [CrossRef]
- 57. Gao, M.; Piao, S.; Chen, A.; Yang, H.; Liu, Q.; Fu, Y.H.; Janssens, I.A. Divergent Changes in the Elevational Gradient of Vegetation Activities over the Last 30 Years. *Nat. Commun.* **2019**, *10*, 2970. [CrossRef]
- 58. Fang, W.; Huang, S.; Huang, Q.; Huang, G.; Wang, H.; Leng, G.; Wang, L.; Guo, Y. Probabilistic Assessment of Remote Sensing-Based Terrestrial Vegetation Vulnerability to Drought Stress of the Loess Plateau in China. *Remote Sens. Environ.* **2019**, 232, 111290. [CrossRef]
- 59. Yao, M.; Li, J.; Zheng, C.; Yao, M.; Zhu, Z. How Predictable Is the Anomaly Pattern of Summer Extreme High-Temperature Days over Central Asia? *Clim. Dyn.* **2024**, *62*, 7651–7664. [CrossRef]
- 60. Wang, C.; Li, Z.; Chen, Y.; Li, Y.; Liu, X.; Hou, Y.; Wang, X.; Kulaixi, Z.; Sun, F. Increased Compound Droughts and Heatwaves in a Double Pack in Central Asia. *Remote Sens.* **2022**, *14*, 2959. [CrossRef]
- 61. Lee, E.; He, Y.; Zhou, M.; Liang, J. Potential Feedback of Recent Vegetation Changes on Summer Rainfall in the Sahel. *Phys. Geogr.* **2015**, *36*, 449–470. [CrossRef]
- 62. Duveiller, G.; Hooker, J.; Cescatti, A. The Mark of Vegetation Change on Earth's Surface Energy Balance. *Nat. Commun.* **2018**, 9, 679. [CrossRef] [PubMed]
- 63. Kong, D.; Miao, C.; Duan, Q.; Lei, X.; Li, H. Vegetation-Climate Interactions on the Loess Plateau: A Nonlinear Granger Causality Analysis. *J. Geophys. Res. Atmos.* **2018**, 123, 11068–11079. [CrossRef]
- 64. Tao, J.; Zhang, Y.; Dong, J.; Fu, Y.; Zhu, J.; Zhang, G.; Jiang, Y.; Tian, L.; Zhang, X.; Zhang, T.; et al. Elevation-Dependent Relationships between Climate Change and Grassland Vegetation Variation across the Qinghai-Xizang Plateau. *Int. J. Climatol.* **2015**, 35, 1638–1647. [CrossRef]

Forests 2025, 16, 1575 31 of 31

65. Chen, X.; Wang, J.; Pan, F.; Huang, B.; Bi, P.; Huang, N.; Gao, R.; Men, J.; Zhang, F.; Huang, Z.; et al. Summer Atmospheric Drying Could Contribute More to Soil Moisture Change than Spring Vegetation Greening. *npj Clim. Atmos. Sci.* **2024**, 7, 296. [CrossRef]

- 66. McDowell, N.; Pockman, W.T.; Allen, C.D.; Breshears, D.D.; Cobb, N.; Kolb, T.; Plaut, J.; Sperry, J.; West, A.; Williams, D.G.; et al. Mechanisms of Plant Survival and Mortality during Drought: Why Do Some Plants Survive While Others Succumb to Drought? New Phytol. 2008, 178, 693–897. [CrossRef]
- 67. Nippert, J.B.; Holdo, R.M. Challenging the Maximum Rooting Depth Paradigm in Grasslands and Savannas. *Funct. Ecol.* **2015**, 29, 739–745. [CrossRef]
- 68. Ivits, E.; Horion, S.; Fensholt, R.; Cherlet, M. Drought Footprint on European Ecosystems between 1999 and 2010 Assessed by Remotely Sensed Vegetation Phenology and Productivity. *Glob. Change Biol.* **2014**, *20*, 581–593. [CrossRef] [PubMed]
- 69. Zhang, Y.; Peng, C.; Li, W.; Tian, L.; Zhu, Q.; Chen, H.; Fang, X.; Zhang, G.; Liu, G.; Mu, X.; et al. Multiple Afforestation Programs Accelerate the Greenness in the "three North" Region of China from 1982 to 2013. *Ecol. Indic.* **2016**, *61*, 404–412. [CrossRef]
- 70. Li, C.; Fu, B.; Wang, S.; Stringer, L.C.; Wang, Y.; Li, Z.; Liu, Y.; Zhou, W. Drivers and Impacts of Changes in China's Drylands. *Nat. Rev. Earth Environ.* **2021**, *2*, 858–873. [CrossRef]
- 71. Micklin, P. The Future Aral Sea: Hope and Despair. Environ. Earth Sci. 2016, 75, 844. [CrossRef]
- 72. Hu, Z.; Zhang, C.; Hu, Q.; Tian, H. Temperature Changes in Central Asia from 1979 to 2011 Based on Multiple Datasets. *J. Clim.* **2014**, 27, 1143–1167. [CrossRef]
- 73. Su, Y.; Chen, S.; Li, X.; Ma, S.; Xie, T.; Wang, J.; Yan, D.; Chen, J.; Feng, M.; Chen, F. Changes in Vegetation Greenness and Its Response to Precipitation Seasonality in Central Asia from 1982 to 2022. *Environ. Res. Lett.* **2023**, *18*, 104002. [CrossRef]

**Disclaimer/Publisher's Note:** The statements, opinions and data contained in all publications are solely those of the individual author(s) and contributor(s) and not of MDPI and/or the editor(s). MDPI and/or the editor(s) disclaim responsibility for any injury to people or property resulting from any ideas, methods, instructions or products referred to in the content.